LA-6723-PR
Progress Report

Special Distribution

Issued: February 1977

Applied Nuclear Data Research and Development

July 1—September 30, 1976

Compiled by

C. I. Baxman
P. G. Young

los alamos
scientific laboratory
of the University of California
LOS ALAMOS, NEW MEXICO 87545

An Affirmative Action/Equal Opportunity Employer

UNITED STATES
ENERGY RESEARCH AND DEVELOPMENT ADMINISTRATION
CONTRACT W-7405-ENG. 36

The four most recent reports in this series, unclassified, are LA-6164-PR, LA-6266-PR, LA-6472-PR, and LA-6560-PR.

This work was performed under the auspices of the Nuclear Regulatory Commission, the National Aeronautics and Space Administration, the Electric Power Research Institute, and the US Energy Research and Development Administration's Divisions of Military Application, Reactor Development and Demonstration, Physical Research, and Magnetic Fusion Energy.

CONTENTS

APPLIED NUCLEAR DATA RESEARCH AND DEVELOPMENT

QUARTERLY PROGRESS REPORT

July 1 - September 30, 1976

Compiled by

C. I. Baxman and P. G. Young

ABSTRACT

This progress report describes the activities of the Los Alamos Nuclear Data Group for the period July 1 through September 30, 1976. The topical content is summarized in the contents.

I. THEORY AND EVALUATION OF NUCLEAR CROSS SECTIONS

A. R-Matrix Analysis of the Four-Nucleon System (G. Hale and D. Dodder [T-9])

The four-nucleon system contains several reactions of interest in applications. The fact that the ^{3}He(n,p)T cross section is quite large and fairly structureless at low energies makes the reaction of some interest as a neutron flux monitor and cross-section standard. The D(d,p)T and D(d,n)^{3}He are important fusion reactions for which it is desirable to have reliable cross-section values at low energies. The four-nucleon system is also of interest theoretically since many of the reactions can be related by charge symmetry or charge independence. The data, therefore, provide a test of the symmetry property of nuclear forces when analyzed in a charge-independent framework.

We have begun a charge-independent R-matrix analysis of reactions in the ^{4}He system at low energies which uses the isospin 1 (T=1) parameters from an earlier analysis of the ^{4}Li system,[1] allowing only a single shift ($\sim$ 400 keV) of the level energies to allow for Coulomb differences between ^{4}He and ^{4}Li. Our present fit, obtained by searching over fewer than 20 T=0 parameters, accounts for most of the measured data available for the T(p,p)T, T(p,n)^{3}He, ^{3}He(n,p)T, and ^{3}He(n,n)^{3}He reactions at energies corresponding to E_p below 5 MeV. The well-established 0^+ resonance at ~20.3-MeV excitation energy, along with its associated threshold effect, shows up clearly in our fits to the T(p,p)T data (see

Fig. 1). In addition, we also confirm the existence of 0^- and 2^- T=0 levels at somewhat higher excitations and see evidence of a second 0^+ and higher 2^+ level above the energy range over which data are currently being analyzed. We expect to obtain firm information about these levels as the energy range of the analysis increases. Figure 2 shows the fits to preliminary new $^1H(t,t)^1H$ cross-section and polarization data[2] taken recently with the Los Alamos Scientific Laboratory (LASL) polarized triton source.

The analysis has just been extended to energies above the d+d threshold, and we expect eventually to be able to describe all the reactions in the four-nucleon system: $^3He(p,p)^3He$, T(n,n)T, T(p,p)T, $T(p,n)^3He$. $^3He(n,n)^3He$, D(d,p)T, $D(d,n)^3He$, and D(d,d)D, in terms of a single set of charge-independent R-matrix parameters.

B. Optical Model Analysis (D. G. Madland, E. D. Arthur, and P. G. Young)

Work has begun on the general problem of developing more realistic optical model potentials for use in nuclear data evaluation and extrapolation. We are studying the feasibility of extracting global optical model parameters on a

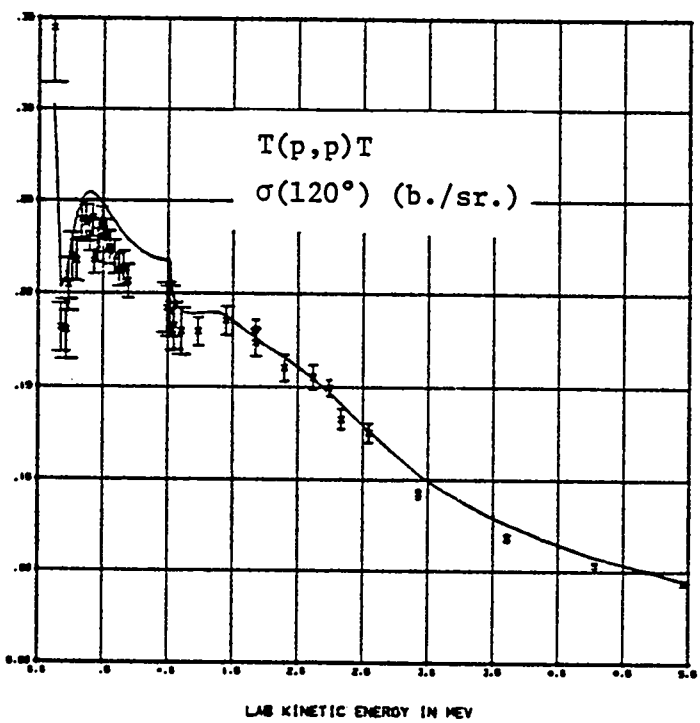

Fig. 1.
Excitation curve for the T(p,p)T differential cross section at θ_{cm} = 120°. The R-matrix calculation (solid curve) is compared to measurements by Jarmie, Ennis, and Haglund.

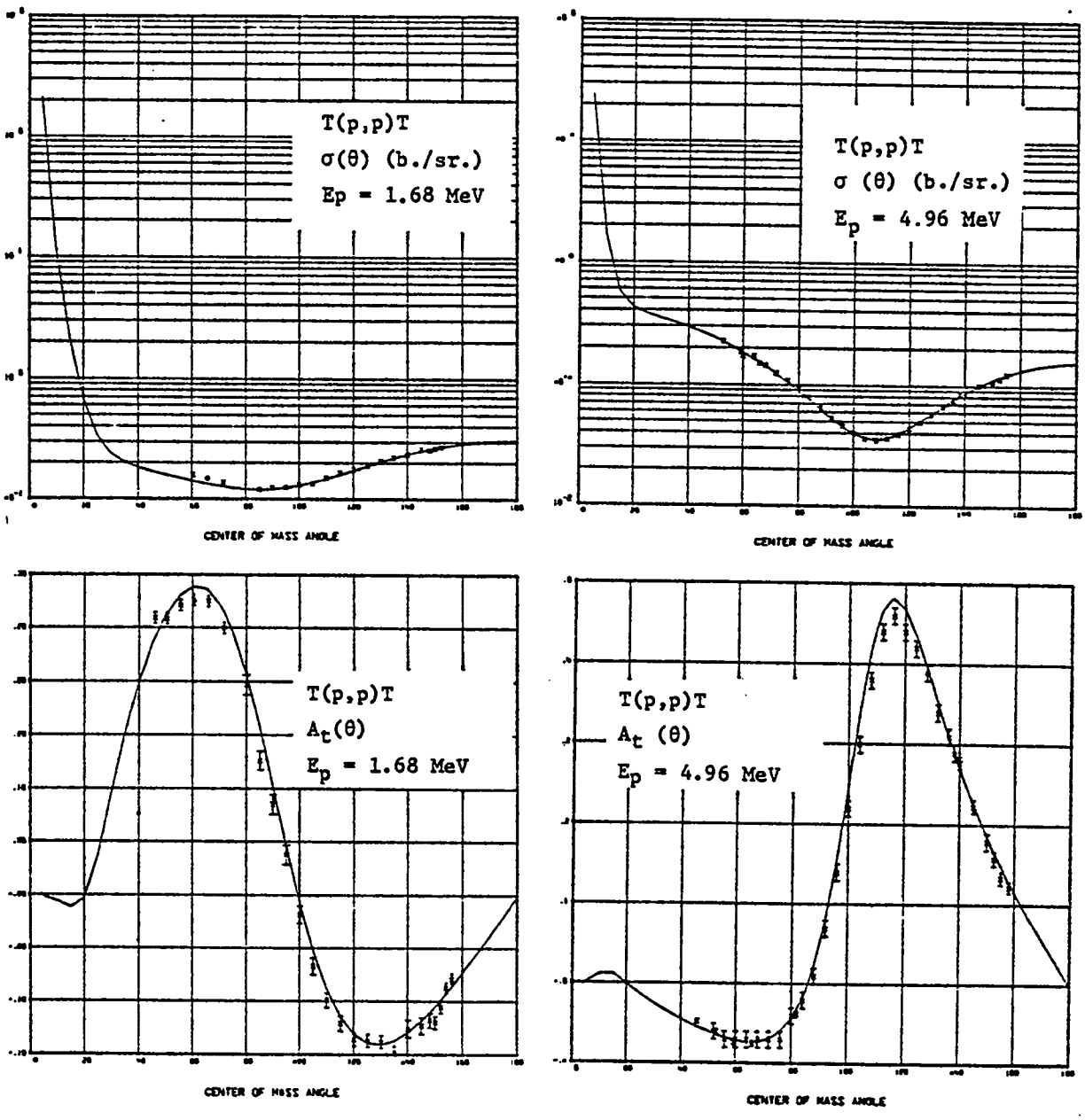

Fig. 2.
Differential cross sections and triton analyzing powers for t-p scattering at proton energies of 1.68 and 4.96 MeV. The data are those of Haglund et al.

shell-by-shell basis, as opposed to the more usual practice of developing a single general set that spans many shells. Specifically, the following items are presently under study (or are planned):

1. The generation of a global neutron-nucleus optical potential for particular shells and for $E_n \leq 40$ MeV.

2. Changes induced in item (1) by the introduction of compound elastic scattering contributions (as a function of neutron energy).

3. Tests and comparisons of the results obtained in items (1) and (2) by using the transmission coefficients generated by the respective potentials in, for example, a number of simple statistical-preequilibrium model calculations using the code GNASH.[3]

We intend to study first the 1p and 1f-2p shells (and initially only the 1p shell) because of the importance of nuclei in this region (A = 5-16, 40-80) in CTR studies.

Items (1) and (2) are being worked on at present. The optical model search code RAROMP[4] (one nucleus/one energy/calculation) has been made operational at LASL and modified to output transmission coefficients directly. Neutron elastic scattering[5] and reaction cross-section[6] data on ^{9}Be at 5.9, 10.1, and 14.2 MeV, as well as data [6,7] on ^{12}C from 8.0 to 14.5 MeV, in 0.5-MeV steps are being studied. The prescription[8] of replacing (1/r) by $(1/r_{so}A^{1/3})$ in the spin-orbit term, which tends to diverge at small r for light nuclei, yields parameter sets that are more consistent with those obtained for heavier nuclei. Whether such parameter sets are more realistic remains to be determined. As expected, the inclusion of compound elastic scattering effects at lower neutron energies dramatically improves the quality of the fits. In the case of ^{9}Be at 5.9 MeV, a factor of 4 improvement in X^2/point was achieved by assuming $\approx$ 20% compound elastic scattering.

The global optical model search code BOMB[9] (several nuclei/several energies/calculation) is being modified to output transmission coefficients in addition to the global parameter sets and will be used for actual production runs in items (1) and (2). Data is expected to be used from the following 1p-shell nuclei: ^{9}Be, ^{10}B, ^{11}B, ^{12}C, ^{14}N, ^{15}N, ^{16}O , and ^{18}O. Note that ^{18}O is already in the 2s-1d shell but has been retained because of the isospin-dependent terms in the potential. The hazard of assuming the existence of optical model parameters with smooth behavior in E_n is recognized (that is, the granularity and low-level density of such light nuclei generally bespeaks a different potential for every

case). Nevertheless, we have decided to begin work in the 1p-shell because a need exists for neutron potentials in this region, especially for neutron energies above 10 MeV. In addition, the 1p shell is good testing ground in the sense that relatively few partial waves are required in the calculations.

After some experience is gained in the 1p shell, we intend to jump to the 1f-2p shell (A = 40-80) where the optical model is known to work much better. In this region use can be made of the fact that the volume integral and mean square radius of the real central potential is well determined from proton-nucleus optical model studies.

C. Coupled-Channel Analysis (D. G. Madland, D. George, and P. G. Young)

The Karlsruhe version[10] of Tamura's coupled-channel elastic-inelastic scattering code JUPITOR[11] has been obtained, changed from IBM-compatible to CDC-compatible, and successfully tested. The LASL version, JUKARL, differs from the Karlsruhe version in that (1) double-precision representation of variable, constants, and functions has been eliminated; (2) certain IBM library functions that are not available on CDC have been replaced with equivalent CDC library functions; (3) portions of blank common have been changed to labeled common; and (4) the feature of renormalization of the wave functions during integration has been deleted because of the larger number representation range available in the CDC-7600. The most stringent test case of Ref. 10 has been reproduced to within the 6th decimal place of the calculated cross sections at back angles. Using a CDC-7600, a full search calculation takes ~20 min for the case of 40-MeV protons on mass 20 targets, with 13 partial waves, spin included, complex coupling, quadrupole and hexadecapole deformations, and no Coulomb-excitation.

This code differs from the original JUPITOR code in two very important respects: (1) an automatic χ^2 minimization search routine has been added, and (2) direct and multiple Coulomb excitation is included.

At present, JUKARL is being modified to output transmission coefficients directly. Once this is complete, the data of Ref. 7 (which includes the 2^+, 4.43-MeV state angular distributions) will be used to calculate transmission coefficients that explicitly account for the presence of this strongly excited, collective state. These transmission coefficients will be compared to those obtained with the optical model (as described above).

D. Calculations of Neutron Capture Cross Sections (E. D. Arthur and P. G. Young)

In response to a request from LASL group TD-6, we have begun calculations of neutron capture cross sections for various isotopes of interest. For low-energy neutron capture, where statistical model calculations can be made, the accurate determination of gamma strength $\frac{2\pi\langle\Gamma_\gamma\rangle}{\langle D\rangle}$ is important in order to reproduce available experimental measurements. We have begun investigation of the systematics in the variation of $\langle\Gamma_\gamma\rangle$ and the observed level spacing $\langle D\rangle$ with mass, and the goodness-of-fit produced by various parameterizations of these quantities when comparisons with experimental data can be made. The study of these systematics will then provide confidence in calculated results for nuclei that have no experimental data.

For higher energy neutron capture where direct or semi-direct effects become important, we have begun to develop a simplified formalism based on a method similar to the calculation of pre-equilibrium particle emission in neutron-induced reactions. In this approach the initial configuration consists of simple particle-hole states. The reaction proceeds through more complicated particle-hole configurations until equilibrium is reached. Preliminary comparisons to available experimental data in the energy range from 8- to 18-MeV incident neutron energy have shown reasonable agreement with spectrum shapes and cross-section magnitudes after determination of normalization parameters.

E. ^{59}Co + n Calculations for Neutron Energies to 40 MeV (E. D. Arthur and P. G. Young)

We have calculated neutron induced reactions on ^{59}Co from 35 keV up to 40 MeV using the pre-equilibrium statistical model code GNASH.[3] These calculations form part of a CSEWG model codes comparison effort (and also provide a test of nuclear model techniques, computer time and cost, etc.) involved in extending nuclear data calculations up to energies required by the CTR program.

For this problem, we used the Moldauer optical model parameters to generate neutron transmission coefficients for energies $\leq$ 1 MeV, while the Wilmore-Hodgson parameters were used to provide neutron transmission coefficients from 1 to 40 MeV. The Becchetti-Greenlees optical parameter sets were used to obtain proton, triton, and helium transmission coefficient sets, while for deuterons and alphas, the Perey and McFadden-Satchler parameters were used, respectively. For gamma-ray transmission coefficients, the Brink-Axel form was used, renorma-

lized to fit a gamma strength of 2.5×10^{-3} at thermal. This same gamma strength was used for all compound nuclei in the calculation.

In the GNASH code all nuclei involved are composed of a discrete level excitation energy region, and above that, a continuum region. Discrete level information and gamma-ray branching ratios were obtained mainly from the Nuclear Data Sheets. For the continuum region, the Gilbert-Cameron level density expression was used with the parameter set of Cook.

The calculation was performed over the following energy intervals with the incident energy step size and the integration bin size shown below:

$0.1 \leq E_n \leq 1$ MeV	E_n varied in 0.1-MeV steps	bin size = .05 MeV
$1.0 < E_n \leq 10$ MeV	E_n varied in 1.0-MeV steps	bin size = 0.1 MeV
$10.0 < E_n \leq 14$ MeV	E_n varied in 2.0-MeV steps	bin size = .25 MeV
$14.0 < E_n \leq 20$ MeV	E_n varied in 2.0-MeV steps	bin size = 0.5 MeV
$20.0 < E_n \leq 40$ MeV	E_n varied in 5.0-MeV steps	bin size = 1.0 MeV

Figure 3 shows the general setup used for the part of the calculation for neutron energies < 20 MeV. Here six compound nuclei are involved and, generally, most energetically allowed reactions (including ones involving t and He^3 emission) were included.

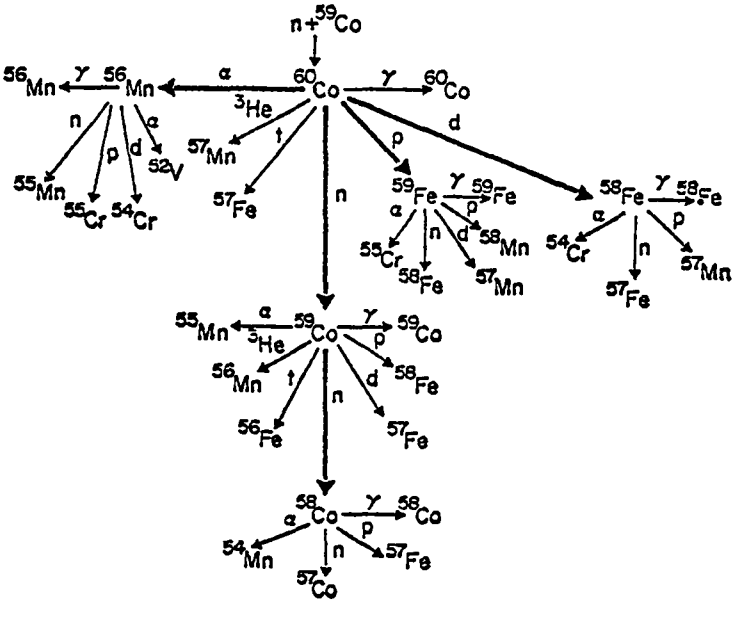

Fig. 3.
Decay chains for $E_n \leq 25$ MeV.

A primary quantity of interest for materials damage studies is the amount of hydrogen or helium produced by neutron induced reactions. For studies involving sources such as $^{7}Li(d,n)$ or $^{9}Be(d,n)$ in which high energy neutrons ($\leqslant$ 40 MeV) can be produced, the number of reactions leading to hydrogen or helium production increases greatly. We thus made one calculation at 30 MeV, involving the decay of 10 compound nuclei, in which major neutron, proton, and alpha decay chains were followed. The allowed decay chains are illustrated in Fig. 4. For this calculation a bin size of 1 MeV was used, and the amount of 7600 computer time used was approximately 5 min. For the remainder of the calculation above 30 MeV, in order to save computer time, we decided to only follow neutron decay chains, allowing gamma-ray, neutron, proton, and alpha emission from each decaying compound nucleus. At 30 MeV the total proton and alpha production cross sections were calculated to be 0.46 and 0.19 b with this more complicated decay scheme; for the simpler scheme, the values were within ~1%. Therefore, the effect of this approximation is negligible.

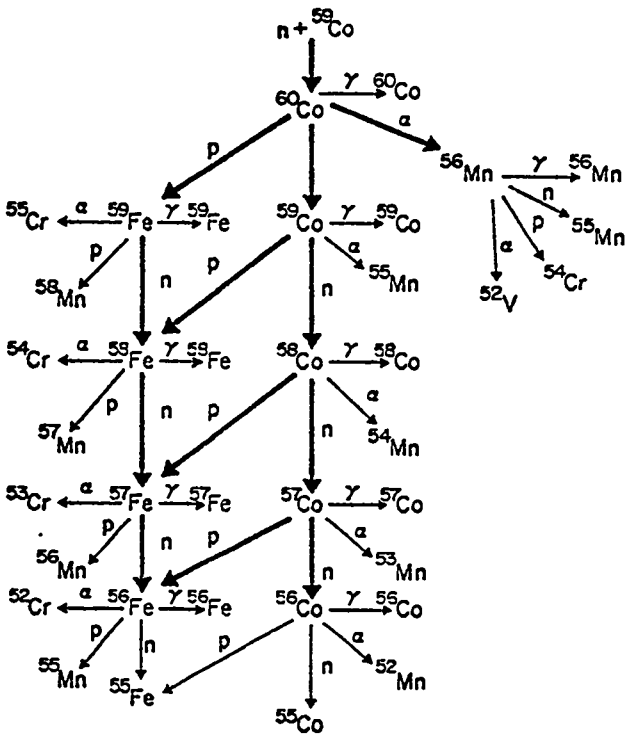

Fig. 4.
Special 30-MeV decay chain.

Figure 5 illustrates the total calculated hydrogen and helium production cross section from 2 to 40 MeV, while Fig. 6 shows the 7600 computer time needed for calculations from 20 to 40 MeV, assuming a bin size of 1 MeV.

F. Multigroup Covariances for ^{27}Al (D. W. Muir, D. G. Foster, Jr., and R. E. MacFarlane)

During this quarter evaluated covariance data were added to the ENDF/B-IV evaluation[12] for ^{27}Al (MAT-1193) and then processed into multigroup form using the ERRORR[13] module of NJOY. The multigroup data are required for the LASL quantitative data assessment for fusion,[14] as well as for other applications. In addition, this exercise provided an opportunity to test both NJOY and the evaluation itself. An interesting and novel feature of the covariance evaluation is the use of the "derived cross-section" formalism with derivation relations that change from one energy region to another.

The coding in the ERRORR module for handling energy-dependent derivation relations was completed some time ago,[13] but this is the first problem executed to test this particular feature. Except for cosmetic changes in the printout,

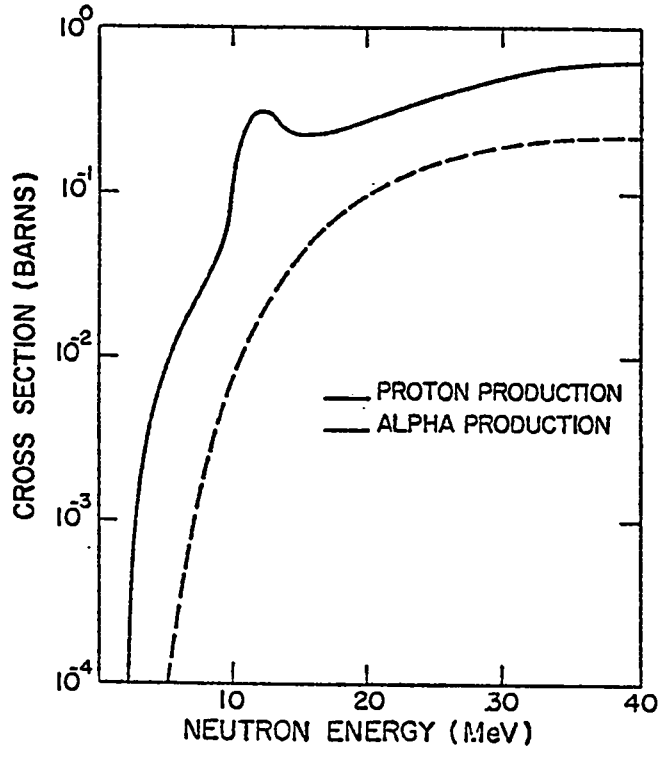

Fig. 5.
Total calculated proton and alpha production cross sections from neutron on ^{59}Co.

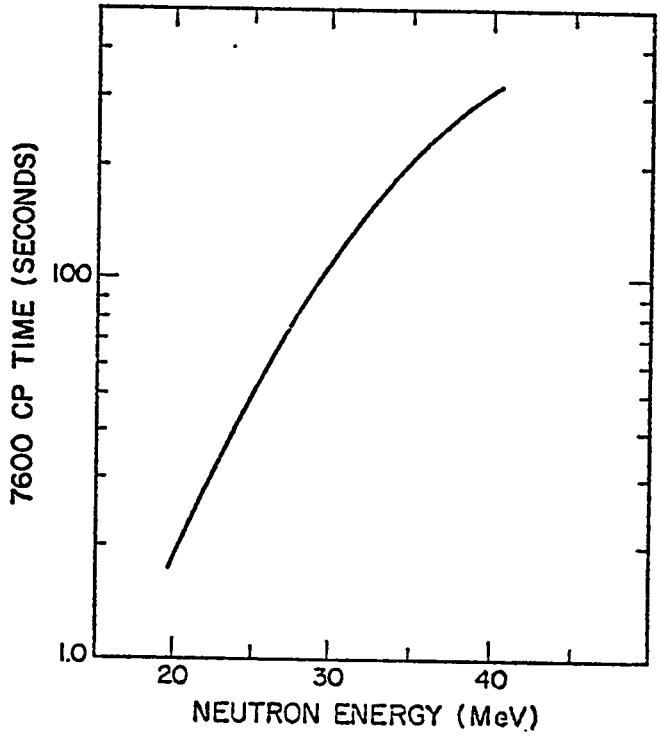

Fig. 6.
7600 CP time needed for n + ^{59}Co using a bin width of 1 MeV.

no changes in the coding were required to process the evaluation successfully. New coding was added to invert the group ordering and write a BCD output file suitable for input to sensitivity analysis codes.

Hand calculations have been performed to compare the multigroup covariances with the uncertainties and correlation structures intended in the ^{27}Al evaluation. Excellent numerical agreement is obtained in all cases examined.

II. NUCLEAR CROSS-SECTION PROCESSING

A. MINX Code Development (R. E. MacFarlane)

The MINX report has been completed and sent to the printer. IBM compatibility changes received from ORNL have been integrated into the master CDC version where possible. Remaining IBM-dependent changes have been collected into one UPDATE deck. The final CDC and IBM versions of MINX have been prepared for return to ORNL and for submission to the Argonne Code Center.

B. NJOY Code Development (R. E. MacFarlane, R. M. Boicourt, and R. J. Barrett)

Three major new capabilities have been added to the NJOY processing system during this quarter: THERMR, which produces thermal scattering cross sections; POWR, which processes multigroup constants into forms used in thermal power reactor analysis; and MATXS, the new generalized CCCC interface file designed for coupled neutron and photon data. These developments are discussed in more detail in other sections of this report.

A systematic testing program has been started which consists of exercising all options, comparisons with existing codes, and comparisons with hand calculations. Many minor errors were discovered and corrected this quarter, especially in rarely used options. This testing program will continue as NJOY is brought up to full production status. An example of this testing and validation is discussed in further detail in Sec. I F.

C. Thermal Scattering Cross Sections (R. E. MacFarlane and R. M. Boicourt)

Accurate and convenient scattering cross sections in the thermal energy range (10^{-5} to 2 eV) are important for the analysis of thermal power reactors. During this quarter we have developed a new NJOY module called THERMR that produces pointwise anisotropic coherent and incoherent cross sections and scattering kernels. The results are in an ENDF-like form that can be converted to multigroup form using the GROUPR module.

Coherent scattering cross sections are produced for several Legendre orders using methods based on HEXSCAT[15] as discussed previously.[16] The pointwise energy grid is determined adaptively so as to represent the cross section to within a specified accuracy by linear interpolation. Constants[17] and form factors are built into the code for graphite, Be, and BeO. The cross sections are written out as sections of File 3 in ENDF/B format. Currently, the P_0 cross section is assigned MT210, P_1 is assigned MT211, etc. The results have been compared with earlier General Atomic (GA) results,[17] and the agreement is excellent.

Incoherent scattering matrices and cross sections can be computed for free atom scattering or for bound atom scattering using $S(\alpha,\beta)$ data in ENDF/B format. In either case,

$$\sigma(E\to E',\mu) = \sigma_f \frac{(A+1)^2}{A^2} \frac{1}{2kT} \sqrt{\frac{E'}{E}}\, e^{-\beta/2}\, S(\alpha,\beta,T) \quad , \tag{1}$$

where $\sigma(E\to E',\mu)$ is the cross section per unit energy and per unit cosine for scattering from E to E' through the angle with cosine μ, σ_f is the free atom scattering cross section, A is the atomic mass ratio of the scattering atom, k is Boltzmann's constant, T is the absolute temperature,

$$\alpha = \frac{E'+E-2\mu\sqrt{EE'}}{AkT} \quad , \tag{2}$$

and

$$\beta = \frac{E'-E}{kT} \quad . \tag{3}$$

For bound atom scattering, $S(\alpha,\beta,T)$ is obtained by interpolating in tables read in File 7 format from existing ENDF/B thermal tapes. For free atom scattering, the scattering function is computed using

$$S(\alpha,\beta,T) = \frac{1}{2\sqrt{\pi\alpha}}\, e^{-\frac{\alpha^2+\beta^2}{4\alpha}} \quad . \tag{4}$$

These calculations require the specification of grids for incident energy, secondary energy, and scattering cosine. In the current version, incident energy and cosine grids are selected arbitrarily. The E' grid is chosen adaptively so as to represent the secondary energy distribution to within a specified tolerance by linear interpolation. The integral of the distribution provides an accurate cross section for each incident energy point that is used to normalize the distribution. Cross sections at intermediate energies are obtained by Lagrangian interpolation.

For bound atom scattering, the cross sections obtained by integration are accurate. However, the formula for free atom scattering [Eq.(4)] was obtained assuming that the scatterer had no internal structure (that is, constant rest-frame cross section). This is certainly not true for a nuclide like ^{240}Pu that has a 10 000-b scattering resonance in the thermal range. In order to preserve the ENDF total and elastic cross sections while still obtaining a reasonable estimate of the scattering distribution, THERMR renormalizes the incoherent cross section to be equal to the Doppler broadened elastic cross section on an input PENDF tape. THERMR then writes the computed or renormalized cross section onto a new PENDF tape using MF3, MT209. The elastic cross section in the thermal range is set to zero, and the total cross section is readjusted if necessary.

In order to represent the normalized scattering kernels on the PENDF tape, we decided to use File 6 (coupled angle-energy distributions). However, an examination of the existing MF6 format[18] showed that it wasn't suitable because it does not allow secondary angle and energy to be closely coupled as required by the kinematics of scattering. Therefore, a new format has been constructed that has incident energy as the outermost loop. This format is more closely compatible with the physics of scattering in both thermal and high-energy problems and is easy to process. The normalized incoherent scattering kernels are written onto the new PENDF tape as MF6, MT209.

The resulting PENDF tape can be processed by subsequent modules of NJOY for group averaging or plotting, or converted to other formats for continuous energy Monte Carlo codes.

D. Cross Sections for Thermal Power Reactor Analysis (R. E. MacFarlane and R. M. Boicourt)

During this quarter we have completed a system for producing cross-section libraries for the new thermal reactor cell depletion code EPRI-CELL.[19] The

scheme is shown in Fig. 7. Data from the ENDF/B general purpose files is used to reconstruct point cross secions in RECONR. The cross sections are accurately Doppler broadened in BROADR, and effective self-shielded cross sections for the unresolved range are added by UNRESR. The resulting pointwise ENDF tape (PENDF) is used as input for the final fast or thermal processing.

For fast data, GROUPR is used to compute multigroup cross sections and scattering matrices in 68 groups. As described previously,[20] the weight function in the epithermal range is computed by solving the integral slowing down equation for mixtures of the isotope desired with hydrogen. The results can be used in equivalence theory to account for mixtures and heterogeneity. A weight function characteristic of mid-life Pressurized Water Reactor (PWR) fuel is used at other energies[16] (with explicit ^{238}U resonance dips removed). The POWR module converts the output of GROUPR into the cross sections, shielding factors, and matrices required by the EPRI-CELL fast library maintenance code GAMTAP.[15] The fast library produced by this sequence has the following special features:

1. Based on ENDF/B-IV.
2. Accurately Doppler broadened.
3. Epithermal self-shielded including broad and intermediate resonance effects.
4. Self-shielded in unresolved range.
5. Flux-weighted fission chi.
6. Multilevel Breit-Wigner resonance capability.

The thermal library sequence starts with the same PENDF tape used for the fast calculation. The THERMR module (see Sec. II C) is used to add coherent and incoherent scattering cross sections and matrices to the PENDF tape. For heavy isotopes, free atom scattering is assumed. Resonance effects are included approximately by renormalizing to the Doppler broadened elastic cross sections from the input PENDF tape. For light moderating isotopes, scattering functions $S(\alpha,\beta)$ are obtained from the ENDF/B thermal tapes. The GROUPR module is used to average the absorption and scattering cross sections on this new PENDF tape using 35 groups and the assumed PWR weighting function. The POWR module is used to reformat the GROUPR output into the form required by the thermal library maintenance code LIBRAR.[15] The thermal library prepared in this way has the following special features:

1. Based on ENDF/B-IV.
2. Cross sections accurately Doppler broadened.
3. Multilevel Breit-Wigner resonance capability available (^{240}Pu).
4. No supplementary resonance parameters required.
5. Multigroup scattering matrices.
6. Absorption + scattering consistent with ENDF/B total cross section.

A preliminary library is being produced containing 20 nuclides and 5 mixtures, with 3 or 4 temperatures each, and with 4 σ_0 values for each heavy isotope.

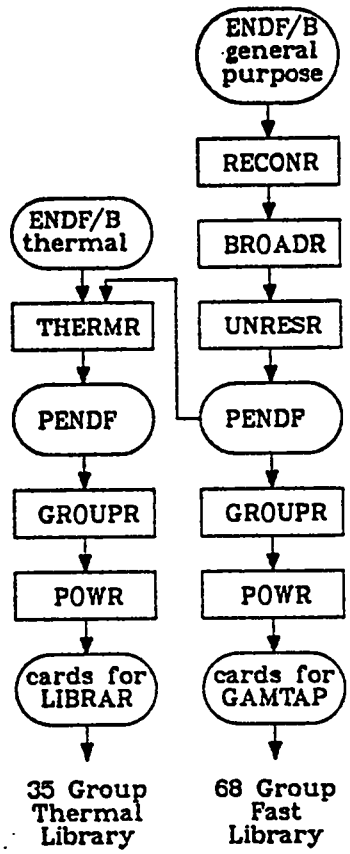

Fig. 7.
Calculational path for producing thermal power reactor cross sections.

E. Comprehensive CCCC Data File: MATXS (R. J. Barrett, H. M. Holleman, and R. E. MacFarlane)

Progress has been made in several areas toward implementing the current version of MATXS. A formatting code has been written and included in the CCCCR module of NJOY. The code will accept (n→n) and (n→γ) group-averaged data from GROUPR and (γ→γ) data from GAMINR. In addition, it will produce all three types of data on the same file in a single computer run. There is virtually no limitation on the number of materials that can be processed in one run, and a different set of materials can be specified for each type of data. As presently written, the code will output all the reactions (MT numbers) that it finds on a given input file. An alternative path, which would allow the user to select the reactions he wants, is under development. Two additional input parameters, IFOPT and NSBLK, allow the user four options as to the size of the matrix records. The options are identical to those available in the ISOTXS format. All of the options have been tested for (n→γ) and (γ→γ) data and checked thoroughly by hand. Only one option has been so tested for the (n→n) data.

A second code, BBC, which translates MATXS data from binary to BCD and from BCD to binary, has been written and thoroughly checked. It is capable of handling all four matrix options described above. The code also has the option of printing selected records from the file.

The ISOTXS to MATXS translator (ITOM) and generalized MATXS printer (PMATXS), both developed during the previous quarter, has been forwarded to the Oak Ridge National Laboratory (ORNL). J. L. Lucius has implemented PMATXS at ORNL with a minimum of difficulty.

F. NJOY Gamma Library (R. J. Barrett)

The calculational tools necessary to produce the gamma-production and gamma-interaction library have been completed during this quarter (see Sec. II E). Preliminary ($n\rightarrow\gamma$) runs have been made on a limited number of isotopes. We have initiated a program to check these results against LAPHANO runs and against hand calculations. An eight-isotopes ($\gamma\rightarrow\gamma$) MATXS file has also been produced and it will also be checked against GAMLEG data.

G. Graphite Scattering Cross Section in the Thermal Region (M. G. Stamatelatos, R. J. LaBauve, R. M. Boicourt, and D. George)

The HEXSCAT code[15] calculates the P_0 and P_1 components of the coherent elastic scattering cross section of polycrystaline materials (e.g., graphite) according to the expression

$$\sigma_\ell = \frac{\sigma_{coh}\,\lambda^2}{2\sqrt{3}\alpha^2 c} \sum_{\tau}^{\frac{\tau}{2\pi} \le \frac{2}{\lambda}} (m_\tau/\tau) f \frac{|F|^2}{N}$$

$$\times \exp\left[-(\hbar^2\tau^2/2M)\right] \int_0^{w_{max}} \rho\frac{(w)}{w} \coth\left(\frac{w}{KT}\right) dw \quad , \tag{5}$$

where

$$f_\ell = 1, \ \ell = 0 \quad (P_0 \text{ component}) \quad , \tag{6}$$

$$f_\ell = \mu, \ \ell = 1 \quad (P_1 \text{ component}) \quad , \tag{7}$$

and

$$\mu = 1 - \frac{\tau^2\lambda^2}{8\pi^2} \quad . \tag{8}$$

We have extended this calculation through the P_5 component of the cross section, that is,

$$f_\ell = P_\ell(\mu) \quad , \quad \ell = 0,1,\ldots 5 \quad . \tag{9}$$

The incoherent inelastic cross section for graphite has been calculated at LASL using the TOR[21] and the GASKET[22] codes. In order to make the two codes perfectly compatible from the output point of view, we have incorporated an option into GASKET to output in exactly the same format as TOR so that both codes can be used interchangeably to generate input data for the GLEN[23] code.

We are also in the process of adapting an IBM version of two British codes, LEAP and ADDELT,[24] to the CDC-7600 computer. LEAP and ADDELT are, in a way, equivalent to TOR and GASKET in that they also calculate the incoherent inelastic cross section for a variety of materials including graphite.

H. Cross Section Generation for Pebble-Bed Reactor Systems (M. G. Stamatelatos and R. J. LaBauve)

This is an independent effort to develop new methods and/or adapt already existing methods for generating shielded cross sections for "pebble-bed" reactor systems of German design. Because of their particular core configuration, the pebble-bed reactor systems require special attention as to the methods for handling the double heterogeneity of fuel-isotope cross sections. The initial core configuration considered was the "reference" design configuration. The neutronics model for this configuration is a three-region core (two concentric cylindrical fuel forms of different ^{235}U enrichment surrounded by a graphite reflector region). The fuel elements consist of well packed spheres (0.61 volume fraction). Each spherical fuel element has a core composed of a mixture of 800-μm-diam. triso fuel grains in a moderator matrix and a spherical reflector shell.

Although new LASL methods for handling the double heterogeneity have already been implemented for the prismatic-fuel cores of High-Temperature Gas Reactors of General Atomic design, significant modifications have been necessary to adapt these and/or other methods to pebble-bed reactor configurations that are considerably different from all other reactors, fast or thermal.

I. Multigroup Cross Sections for Design of the Intermediate Spectrum Neutron Facility (D. W. Muir and R. J. LaBauve)

This quarter we performed a series of calculations in support of the design of the Intermediate-Energy Standard Neutron Field (ISNF) to be located at the National Bureau of Standards (NBS). This facility consists of a spherical cavity in a graphite thermal column. Lining the cavity is a thin foil of ^{235}U. Thermal neutrons produce fissions in the ^{235}U, and the resulting fission-spectrum neutrons (plus neutrons reflected by the graphite) provide the desired intermediate-energy neutron spectrum at the center of the cavity. We are preparing a 53-group set of cross sections to be used in subsequent discrete-ordinates and multigroup Monte Carlo calculations at NBS.

The 53-group set will be produced by performing a space-dependent collapse from the T-2 240-group library.[25] As part of this task we have performed detailed neutron flux calculations on a one-dimensional model of the ISNF, shown in Table I. These calculations were performed using a newly developed version[26] of the ONETRAN code[27] that is especially designed to handle very large group structures.

It is expected that the minimum in ^{12}C at 6.6 MeV will present a significant streaming path to the neutrons in the graphite reflector. This is borne out by an examination of the 240-group leakage spectrum in that energy region, as shown in Table II. It is interesting to note that the factor-of-two structure in σ_{tot} results in roughly a factor-of-ten enhancement of the leakage per unit lethargy in the minimum. From this, it is clear that streaming in this minima is not handled at all well by the infinite-medium Bondarenko flux model often used to produce self-shielded cross sections. This model assumes that

$$\phi(E) = \frac{1}{\sigma_{tot}(E)}$$

for a homogeneous, single material. The maximum in σ_{tot} for ^{27}Al can also be seen to have some noticeable effects in Table III. This maximum reduces the flux by a factor of two.

TABLE I

ISNF ONE-DIMENSIONAL MODEL

Outer Radius of Spherical Shell (cm)	Atomic Densities 10^{24} cm^{-3}
5.838	Void
7.131	$^{10}B(0.05865)$ + $^{12}C(0.00383)$ + $^{27}Al(0.02215)$
7.2005	$^{27}Al(0.06029)$
15.0	Void
65.0	$^{12}C(0.08695)$

TABLE II

NET LEAKAGE NEAR 6.6-MeV ^{12}C MINIMUM

IG	E_{low} (MeV)	Δu	L(IG)	L(IG) x $\frac{0.025}{\Delta u}$	σ_{tot} (IG)
39	7.596-7.788	0.025	6.45-6	6.45-6	1.999
40	7.408	0.025	6.90-6	6.90-6	1.782
41	7.225	0.025	1.79-5	1.79-5	1.419
42	7.047	0.025	1.19-4	1.19-4	0.769
43	6.873	0.025	1.39-4	1.39-4	0.744
44	6.703	0.025	1.39-4	1.39-4	0.790
45	6.648	0.0083	4.30-5	1.29-4	0.859
46	6.592	0.0083	5.36-5	1.61-4	0.807
47	6.538	0.0083	5.78-5	1.73-4	0.806
48	6.376	0.0025	1.01-5	1.01-4	1.091
49	6.219	0.025	3.71-5	3.71-5	1.825
50	6.065	0.025	7.18-5	7.18-5	1.174
51	5.916	0.025	8.33-5	8.33-5	1.109

TABLE III

CENTRAL FLUENCE NEAR 35-keV ^{27}Al MAXIMUM

IG	E_{low} (keV)	Δu	ϕ(IG)	$\phi(IG) \times \frac{0.025}{\Delta u}$	σ_{tot} (IG)
163	46.31-52.48	0.125	1.36-5	2.72-6	2.68
164	40.87	0.125	1.25-5	2.50-6	4.21
165	36.07	0.125	9.96-6	1.99-6	12.59
166	35.18	0.025	1.35-6	1.35-6	32.14
167	34.31	0.025	1.39.6	1.39-6	33.18
168	31.83	0.075	6.72-6	2.24-6	14.09
169	28.09	0.125	1.26-5	2.52-6	1.95

III. INTEGRAL TESTING OF METHODS AND DATA -- Packaged Benchmarks for Reference Calculations and Integral Testing (R. B. Kidman)

A project to set up codes and computer decks for the Cross Section Evaluation Working Group (CSEWG) reactor benchmarks[28] is nearing completion. The general approach is to form one complex deck (packaged benchmark) for each critical assembly that will generate practically all calculated data of conceivable interest.

The reasoning behind this approach is to provide a powerful analytical tool that can conveniently and completely test the effect of any data or method change on every aspect of any critical assembly with a simple submittal of a single deck. Thus, each packaged benchmark is composed of the following runs:

1. 1DX[29] - 1-D diffusion theory central activities.
2. 1DX - 1-D diffusion theory flux and effective cross sections.
3. 1DX - 1-D diffusion theory adjoint.
4. PERTV[30] - 1-D diffusion theory worths, delayed neutron fraction, neutron generation time, and inhour/δK conversion factor.
5. 2DB[31] - 2-D diffusion theory flux.
6. 2DB - 2-D diffusion theory adjoint.
7. PERTV - 2-D diffusion theory worths, delayed neutron fraction, neutron generation time, and inhour/δK conversion factor.
8. 1DX - Effective cross sections for use in transport theory.
9. ONETRAN[27] 1-D transport theory flux.
10. ONETRAN - 1-D transport theory adjoint.
11. PERTV - 1-D transport theory worths, delayed neutron fraction, neutron generation time, and inhour/δK conversion factor.

Each packaged benchmark calculates experimentally measured quantities in 1-D and 2-D diffusion theory and in 1-D transport theory. Hence, we have available 1-D to 2-D to transport theory adjustment factors for every parameter.

This system is currently being debugged with the LIB-IV[16] cross-section library. This will also establish a set of reference calculations that will be documented. The effects of any changes can be measured against this reference set. Since all fluxes, adjoints, and cross sections are being saved for each benchmark, detailed individual or collective investigations and/or comparisons can be carried out in the future. Some preliminary uncorrected 1-D diffusion theory eigenvalues are shown in Table IV.

Experience has shown that unless testing can be made trivially easy to do, it will not be done at all or done in an incomplete fashion. This is why we are stressing the need for convenience of testing (even the computer output is conveniently stored on microfiche) and why we feel the packaged benchmark concept is potentially very useful.

TABLE IV

1-D DIFFUSION THEORY EIGENVALUES
USING LIB-IV

	Benchmark	Uncorrected k_{eff}
1	JEZEBEL	0.94850
2	VERA-11A	0.94486
3	ZPR-3-48	0.97584
4	ZEBRA-3	0.99456
5	GODIVA	0.97437
6	VERA-1B	0.97410
7	ZPR-3-6F	0.99756
8	ZPR-3-11	1.00893
9	ZPR-3-12	0.99758
10	ZEBRA-2	0.99084
11	ZPPR-2	0.97293
12	ZPR-6-7	0.97085
13	ZPR-3-56B	0.95572
15	ZPR-6-6A	0.98343
16	SNEAK-7A	0.98633
17	SNEAK-7B	0.93731

IV. FISSION-PRODUCT YIELD AND DECAY DATA STUDIES

A. Recent Comparisons of Decay Spectra, Heating, and Absorption Effects (T. R. England, M. G. Stamatelatos, W. B. Wilson, and N. L. Whittemore)

1. Neutron Absorption Effect on Decay Heating. Calculations of absorption effects on decay heating for thermal fission of ^{235}U and ^{239}Pu were performed for presentation to the ANS 5.1 Standards Subcommittee. The results are shown in Figs. 8-13. (Note that for each case two plots are given covering different time domains.) The effect is dependent on the flux time, flux level, irradiation, and cooling time. The dominant effect results from neutron absorption in ^{133}Cs that produces the shielded nuclide ^{134}Cs. This is relatively easy to parameterize; it can, in fact, be represented by a simple two-element chain, or its equivalent, and does not require an approximation. This particular effect is dependent on the neutron spectrum and particularly on the ratio of the epithermal-to-thermal flux levels and flux time.

The remaining absorption effect is small for moderate flux levels and requires no complex approximation. The calculations were performed as follows:

1. Four-group cross sections were processed from ENDF/B-IV files using T = 900°F and a mid-life spectrum. (The spectrum was generated using inventories supplied by Westinghouse.)
2. An irradiation time of 20 000 h was used.
3. $\phi_{th} = 10^{13}$ was applied to an effective 2200-m/s cross section,

$$\sigma_{eff} \equiv \frac{\bar{\sigma}}{\bar{\sigma}_{1/v}} ,$$

where $\bar{\sigma}$ is averaged in the LWR spectrum, and $\bar{\sigma}_{1/v}$ is a 1/v cross section averaged in the same spectrum ($\bar{\sigma}_{1/v} = 0.55402$ in this spectrum) having a value of 1 b at 0.0253 eV; therefore, σ_{eff} is approximately the 2200-m/s value except for any non-1/v dependence.
4. The total flux in the resonance region was 5×10^{13} (over the energy range 0.625-5530 eV). The 2 fast flux values were 6×10^{13} and 8×10^{13} over the ranges 5530 to 8.21×10^5 and 8.21×10^5 to 10^7 eV, respectively. The fast group fluxes are of minor importance in thermal reactors.
5. One case increased the flux levels by ten to evaluate the effect of increased flux time.
6. Fuel was not permitted to deplete in any calculation.
7. The above fluxes apply to cases where neutron absorption is permitted. The cases without neutron absorption used fluxes reduced to 10^4.

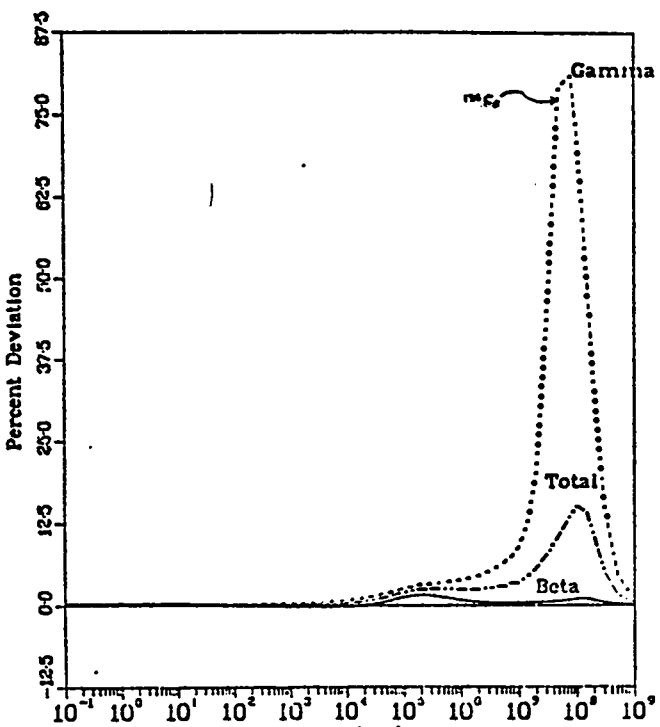

Fig. 8.
Percent deviation of decay heating due to neutron absorption (^{235}U irradiation for 20 000 h, no depletion) ($\phi = 10^{13}$).

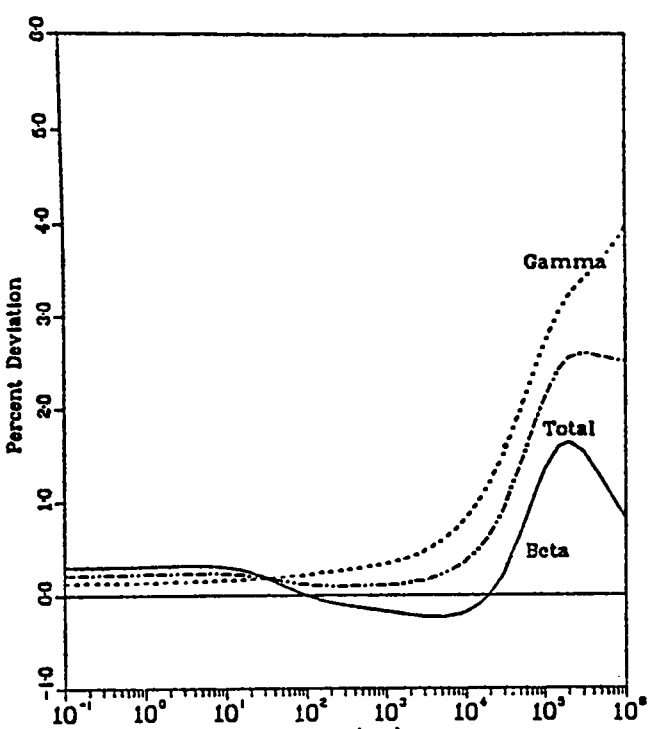

Fig. 9.
Percent deviation of decay heating due to neutron absorption (^{235}U irradiation for 20 000 h, no depletion) ($\phi = 10^{13}$).

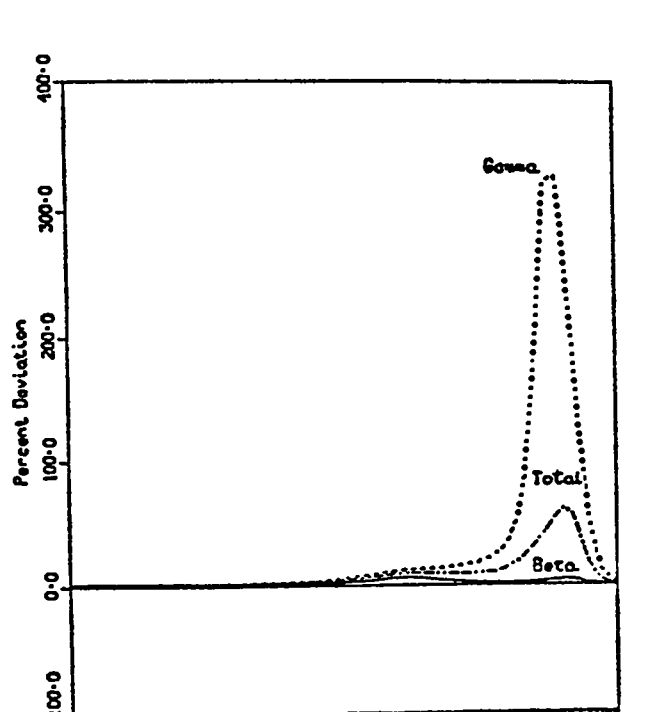

Fig. 10.
Percent deviation of decay heating due to neutron absorption (^{235}U irradiation for 20 000 h, no depletion) ($\phi = 10^{14}$).

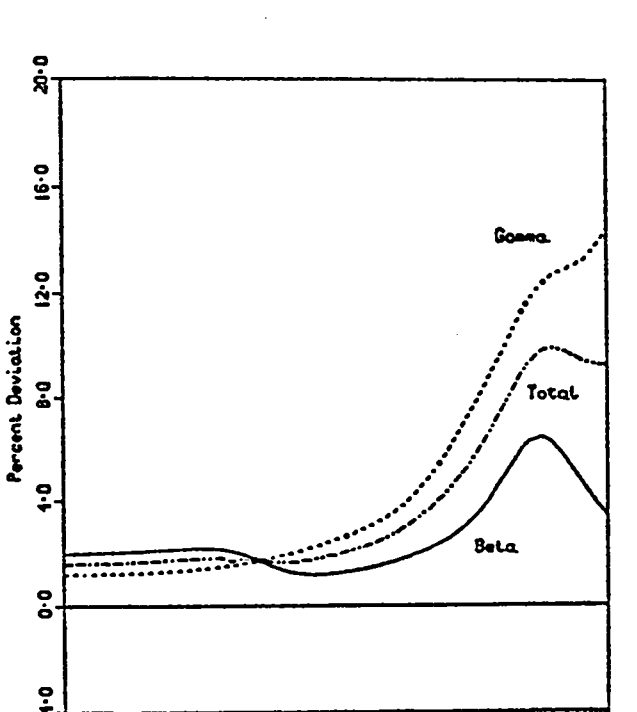

Fig. 11.
Percent deviation of decay heating due to neutron absorption (^{235}U irradiation for 20 000 h, no depletion) ($\phi = 10^{14}$).

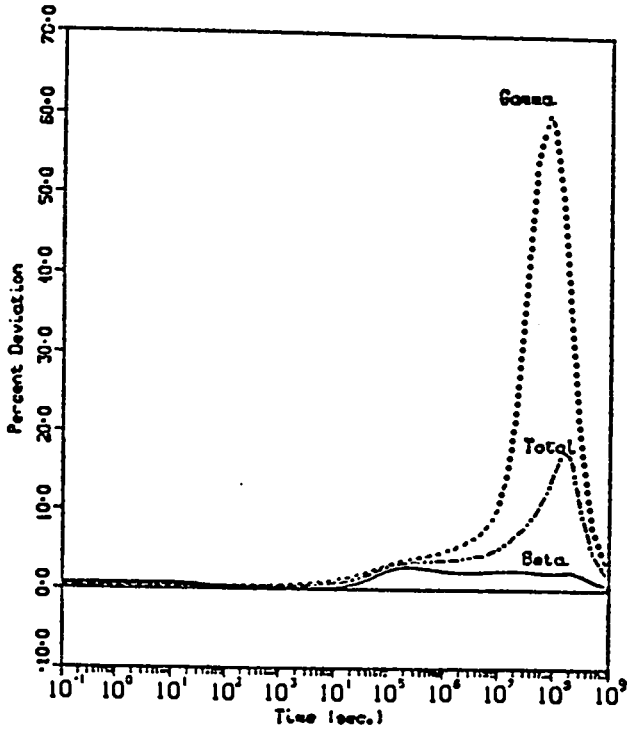

Fig. 12.
Percent deviation of decay heating due to neutron absorption (^{239}Pu irradiation for 20 000 h, no depletion) ($\phi = 10^{13}$).

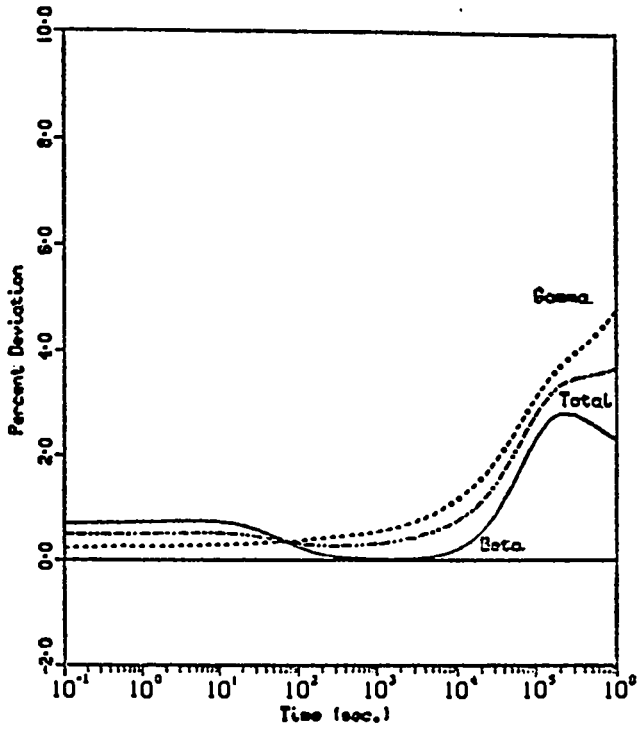

Fig. 13.
Percent deviation of decay heating due to neutron absorption (^{239}Pu irradiation for 20 000 h, no depletion) ($\phi = 10^{13}$).

2. Recent Comparisons of Summation Calculations with β and γ Spectra and Total Decay Heating. Figures 14-22 show comparisons of calculated gamma spectra with Jurney's (LASL) most recent measurements. The plots are actually histograms with 50-keV wide bins. Note that energy (MeV/fis), not photon multiplicity, is compared. This emphasizes the high energy range. Also, MeV/fis refers to the energy per bin.

Table V shows a comparison of integrated gamma energy. An earlier pilot experiment showed even better overall agreement with calculations. At long cooling times, this comparison is also included.

Comparisons of calculated beta spectra with the experiments of Tsoulfanidis[32] are shown in Figs. 23-29. Integrated comparisons are given in Table VI. Again, the plotted points are histogram values; for β spectra, 75 groups (100 keV wide) were used and the MeV/fis refers to the energy per bin. Note that the irradiation times in the gamma and beta comparisons were comparable (28 800 s for β and 20 000 s for γ).

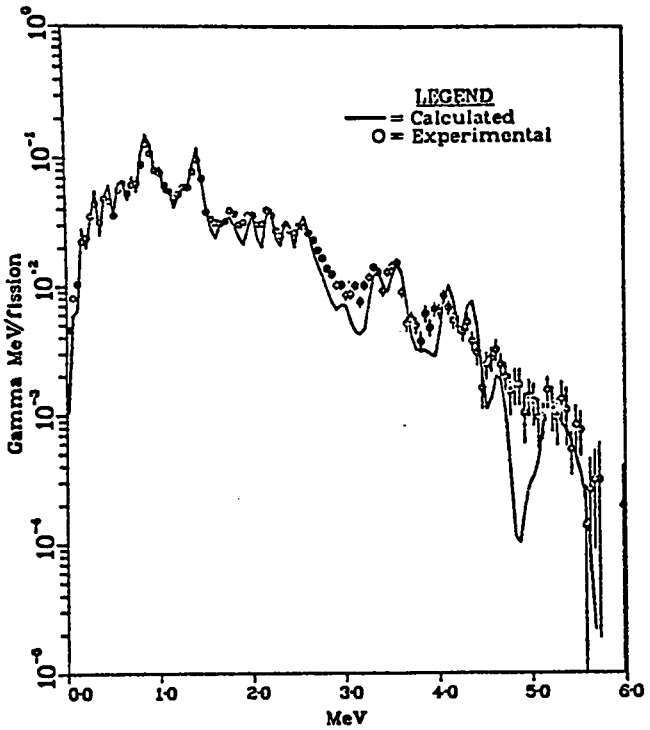

Fig. 14.
Fission-product gamma MeV/fission/bin at 5.56-h irradiation and 70 s-cooling

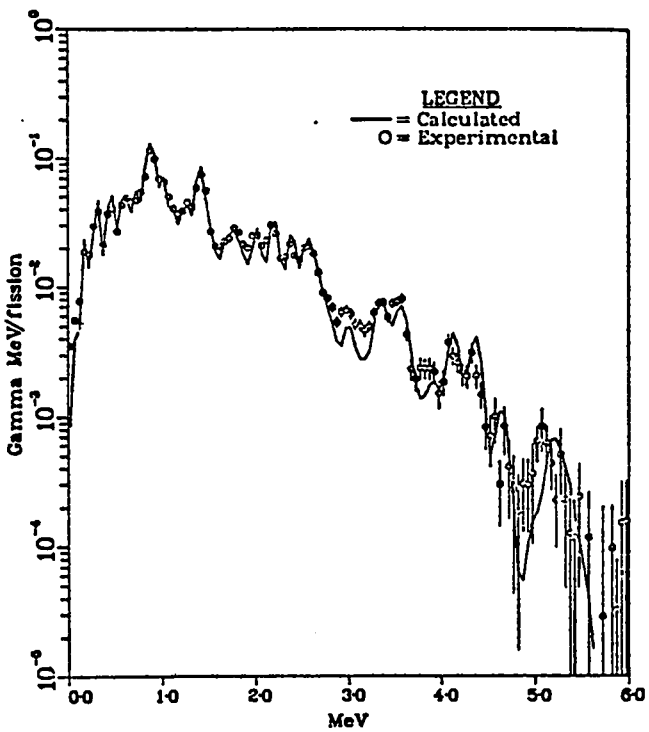

Fig. 15.
Fission-product gamma MeV/fission/bin at 5.56-h irradiation and 199-s cooling.

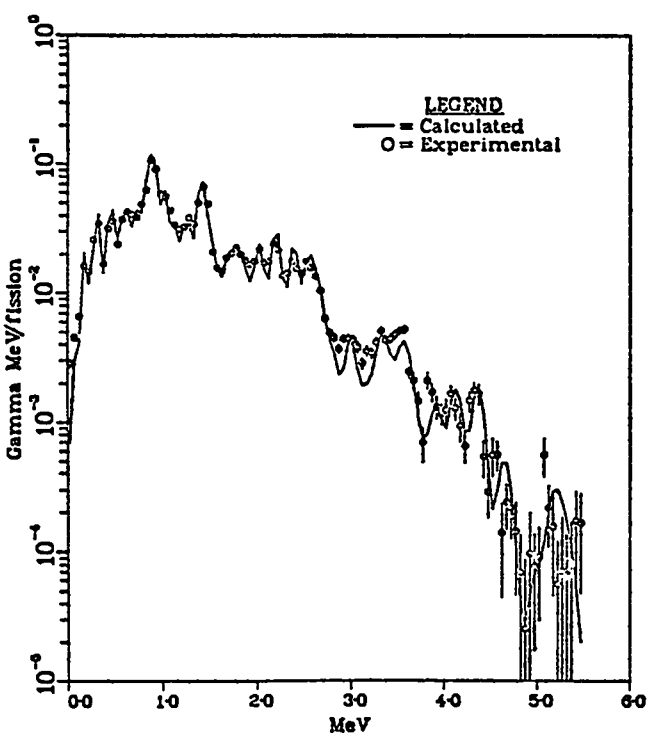

Fig. 16.
Fission-product gamma MeV/fission/bin at 5.56-h irradiation and 388-s cooling.

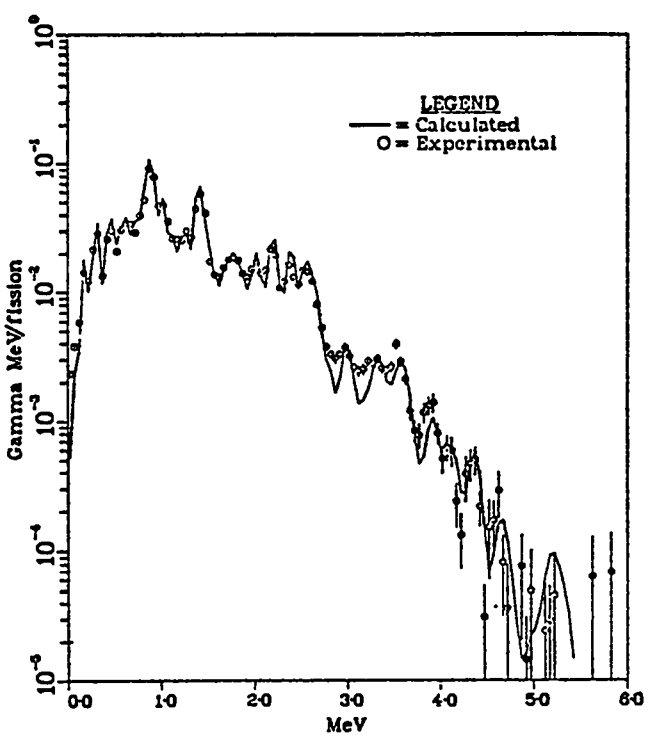

Fig. 17.
Fission-product gamma MeV/fission/bin at 5.56-h irradiation and 660-s cooling.

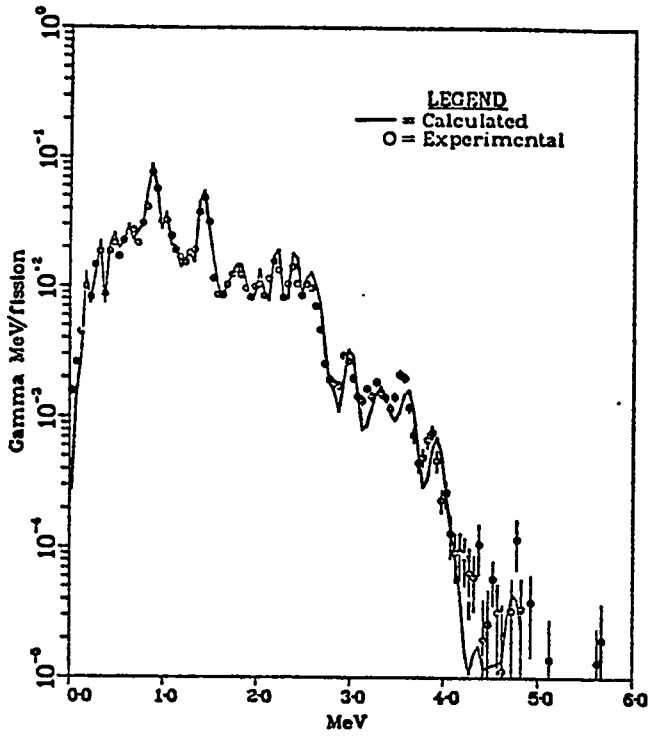

Fig. 18.
Fission-product gamma MeV/fission/bin at 5.56-h irradiation and 1524-s cooling.

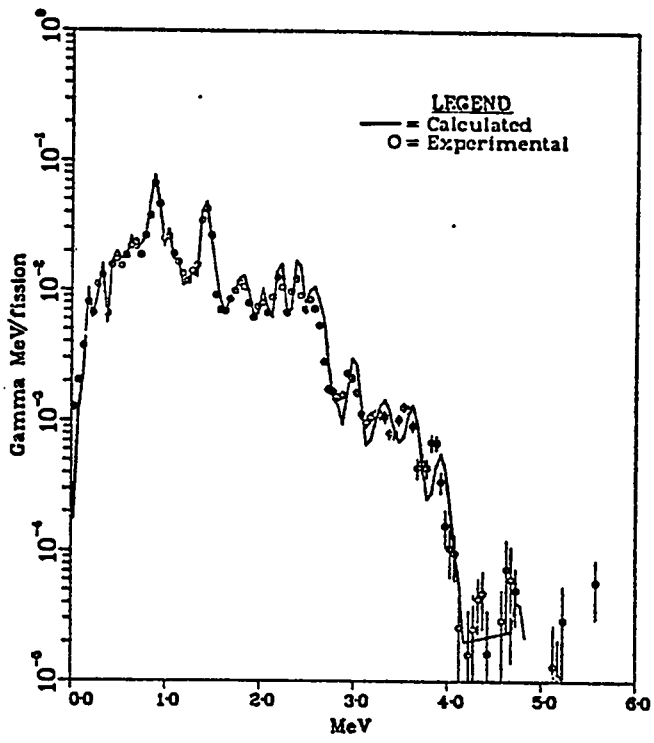

Fig. 19.
Fission-product gamma MeV/fission/bin at 5.56-h irradiation and 2214-s cooling.

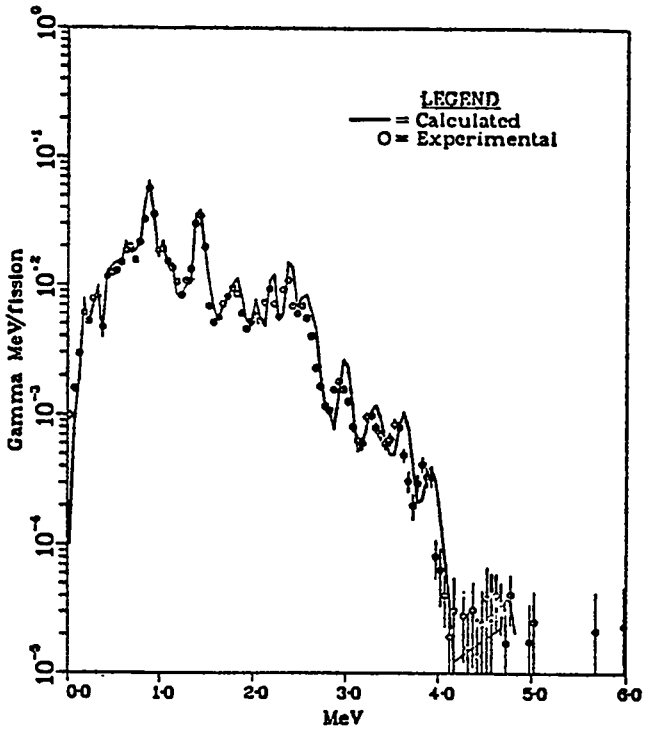

Fig. 20.
Fission-product gamma MeV/fission/bin at 5.56-h irradiation and 3234-s cooling.

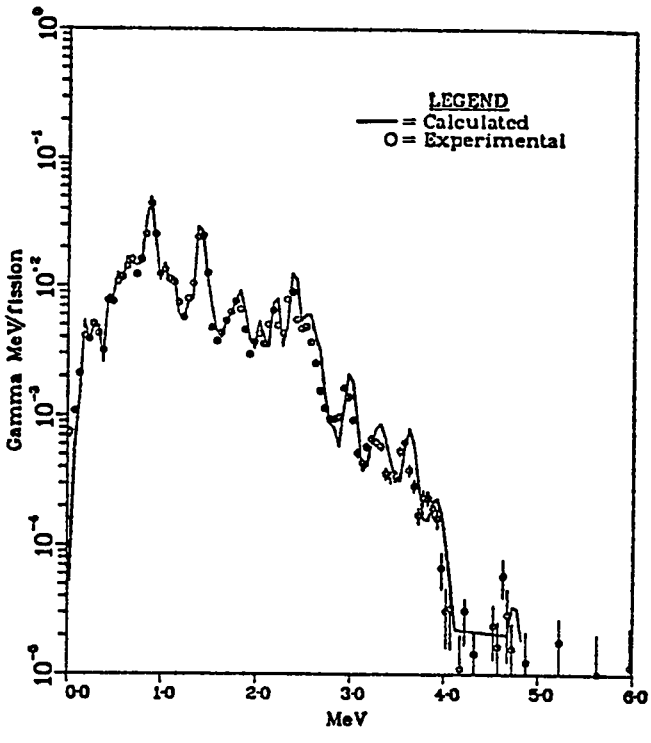

Fig. 21.
Fission-product gamma MeV/fission/bin at 5.56-h irradiation and 5000-s cooling.

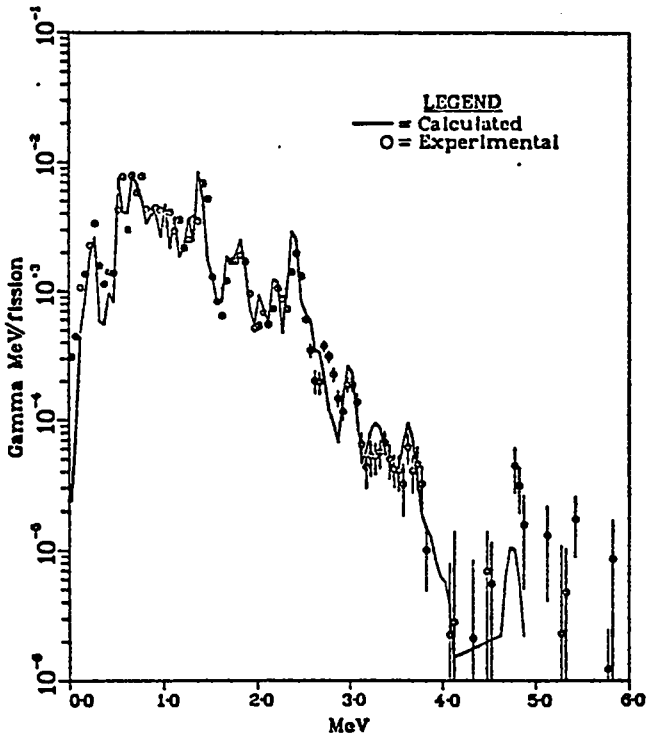

Fig. 22.
Fission-product gamma MeV/fission/bin at 5.56-h irradiation and 21845-s cooling.

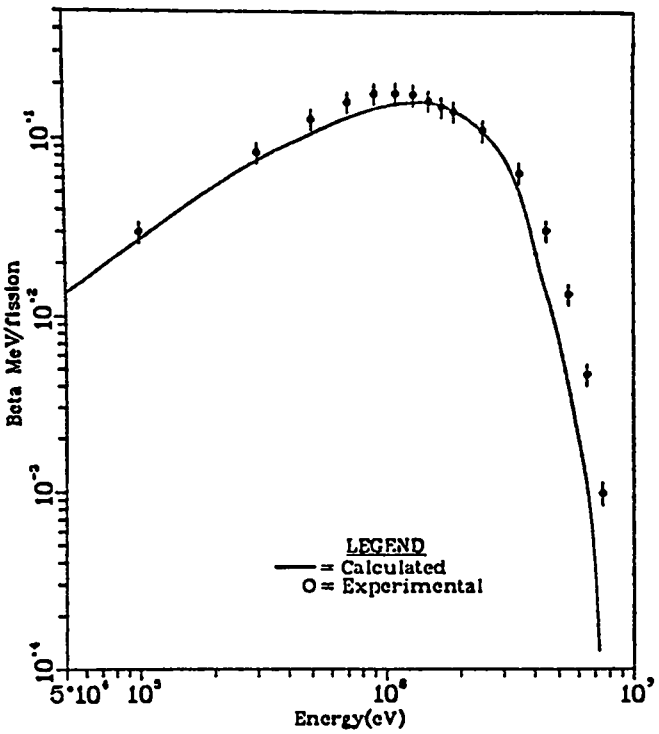

Fig. 23.
Beta MeV/fission at 8-h irradiation and 6-s decay.

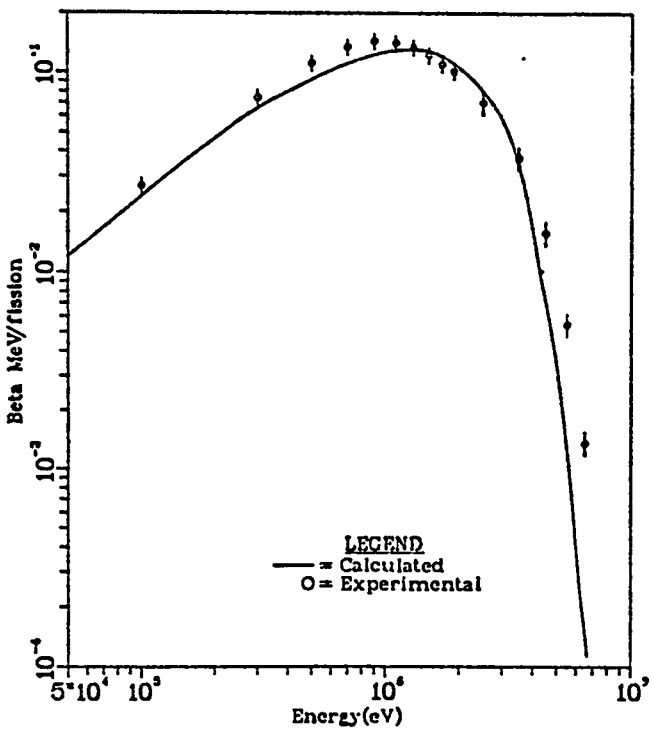

Fig. 24.
Beta MeV/fission at 8-h irradiation and 21-s decay.

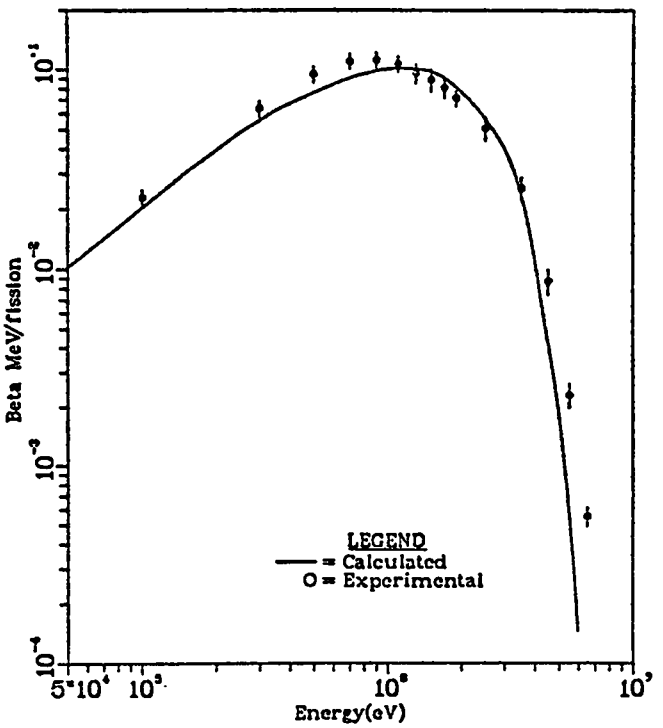

Fig. 25.
Beta MeV/fission at 8-h irradiation and 66-s decay.

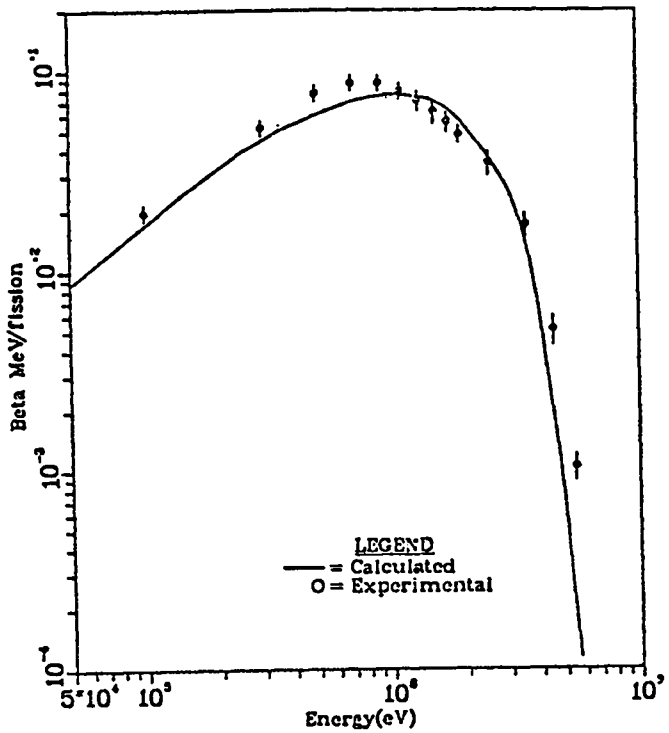

Fig. 26.
Beta MeV/fission at 8-h irradiation and 210-s decay.

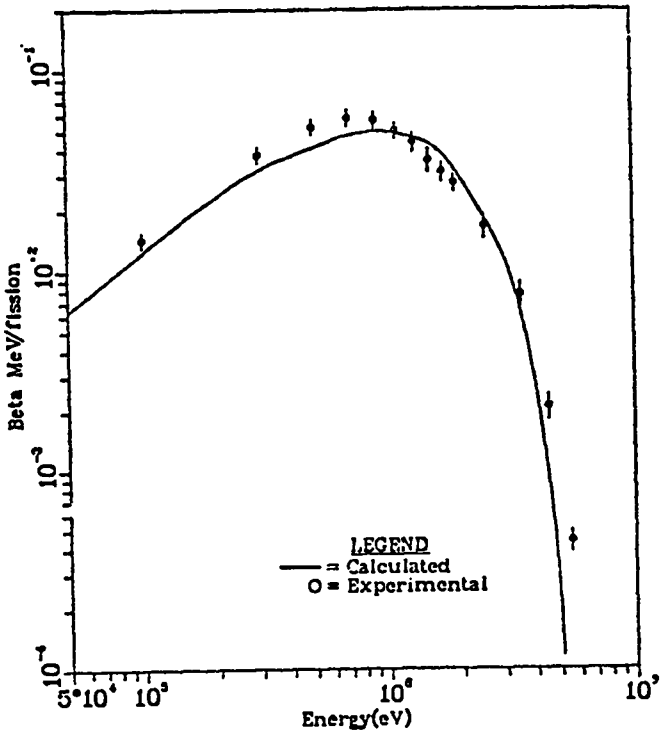

Fig. 27.
Beta MeV/fission at 8-h irradiation and 960-s decay.

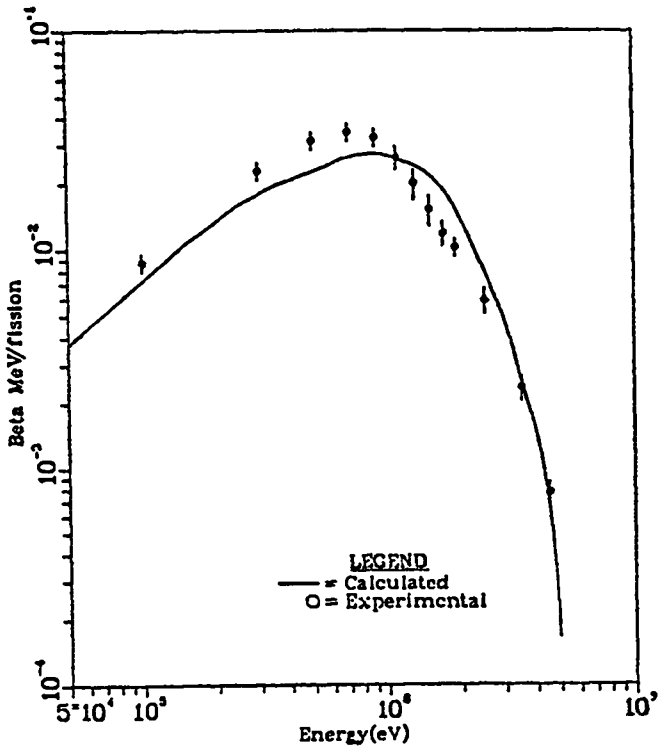

Fig. 28.
Beta MeV/fission at 8-h irradiation and 3750-s decay.

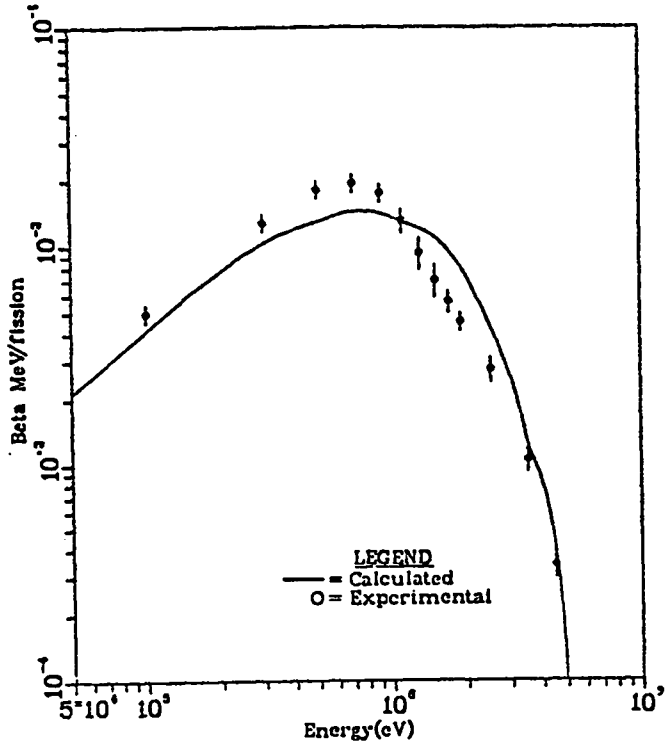

Fig. 29.
Beta MeV/fission at 8-h irradiation and 10950-s decay.

TABLE V

COMPARISON OF CALCULATED INTEGRATED GAMMA RELEASE RATES WITH LASL EXPERIMENT[a]

Mean Cooling Time (s)	MeV/Fiss Experimental	-----% Difference----- (C-E)/E Including IC	Excluding IC	% Energy Due to Nuclides Having Spectra
70	2.741	- 0.86	- 1.10	87.6
199	2.058	+ 0.22	- 0.07	93.5
388	1.724	+ 0.03	- 0.29	95.5
660	1.429	+ 3.84	+ 3.47	96.6
1524	1.021	+ 7.70	+ 7.26	98.0
2214	0.8422	+ 9.14	+ 8.65	98.7
3234	0.6712	+ 9.97	+ 9.43	99.3
5000	0.4981	+ 9.46	+ 8.85	99.7
21845	0.1328	- 3.45	- 4.72	99.8
EARLIER RESULT FROM PILOT EXPERIMENT[b]				
62136	0.03518	+ 7.8	+ 5.3	99.9
151200	0.01216	+ 8.4	+ 4.5	99.8

[a] Unpublished 1976 experiments by E. Jurney, LASL. ^{235}U thermal fission following 20 000-s irradiation.

[b] The shorter cooling time comparison with E. Jurney's pilot experiment is not believed to be as accurate as the two long cooling times listed. (However, the overall agreement with calculations was closer than the above values and did not exhibit the above disparity between 1524 and 5000 s.)

The LASL calorimetric experiment for total decay heating (Yarnell, LASL) and the comparisons with calculations (including corrections for gamma escape, experimental details, and estimated uncertainties) are essentially complete. Table VII and Fig. 30 show the final results of this important experiment. (Results are based on three samples.) The uncertainty (1σ) of the experiment after ~20 s is ~2.5%.

TABLE VI

COMPARISON OF CALCULATED INTEGRATED BETA RELEASE RATES WITH EXPERIMENT[a]

Mean Cooling Time (s)	Experimental MeV/Fiss	% Difference (C-E)/E	% Energy Due to Nuclides Having Spectra
6	4.976	-13.8	67.8
21	3.513	- 4.9	75.2
66	2.582	- 3.2	82.9
210	1.7715	- 5.2	92.3
960	1.089	- 3.2	97.1
3750	0.518	+ 3.4	99.2
10950	0.267	+ 6.0	99.7

[a]Experimental values are in Ref. 32. Values listed follow an irradiation of 28 800 s.

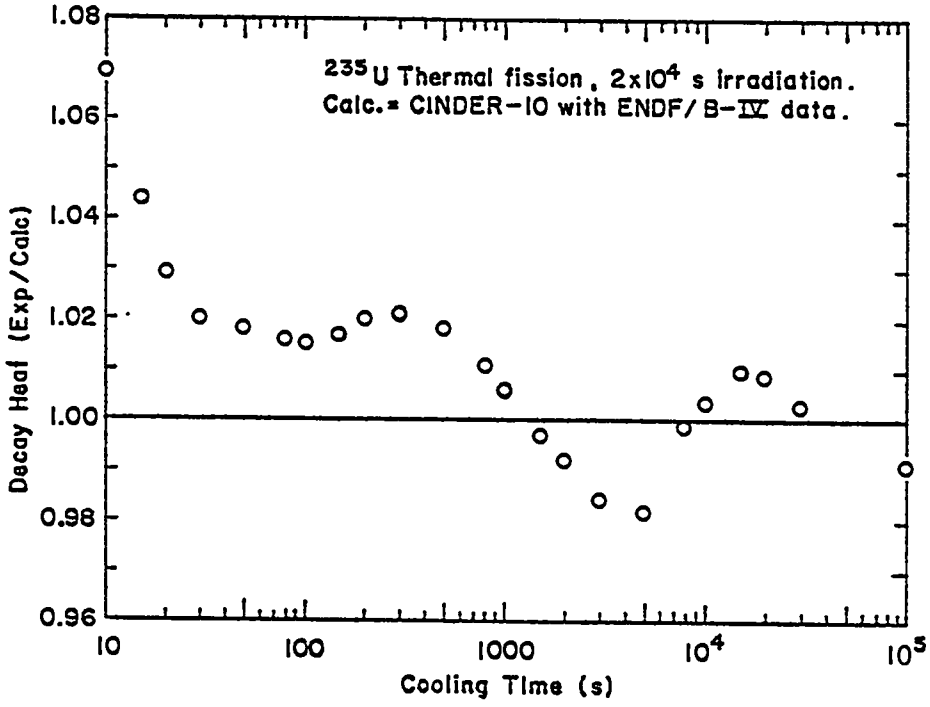

Fig. 30.
Comparison of total decay heating (J. Yarnell's calorimetric experiment with calculations).

TABLE VII

COMPARISON: CALCULATED TOTAL DECAY HEATING WITH PRELIMINARY LASL MEASUREMENTS (J. Yarnell, LASL P-2)

COOLING TIME (s)	CALORIMETER (MEV/FISS)	GAMMA ESCAPE (MEV/FISS)	TOTAL DECAY HEAT (MEV/FISS)	CALC. DECAY HEAT (MEV/FISS)	DECAY HEAT (EXP./CALC.)
10	8.078	0.240	8.318	7.780	1.069
15	7.336	0.221	7.557	7.239	1.044
20	6.835	0.207	7.042	6.842	1.029
30	6.212	0.189	6.401	6.276	1.020
50	5.498	0.164	5.662	5.562	1.018
80	4.854	0.141	4.995	4.915	1.016
100	4.560	0.130	4.690	4.619	1.015
150	4.071	0.112	4.183	4.112	1.017
200	3.755	0.101	3.856	3.780	1.020
300	3.338	0.088	3.426	3.355	1.021
500	2.852	0.073	2.925	2.873	1.018
800	2.421	0.061	2.482	2.455	1.011
1000	2.216	0.056	2.272	2.258	1.006
1500	1.849	0.046	1.895	1.901	0.997
2000	1.596	0.040	1.636	1.650	0.992
3000	1.259	0.031	1.290	1.311	0.984
5000	0.8974	0.0222	0.9196	0.9362	0.982
8000	0.6400	0.0149	0.6549	0.6553	0.999
10000	0.5344	0.0120	0.5464	0.5440	1.004
15000	0.3740	0.0077	0.3817	0.3778	1.010
20000	0.2847	0.0054	0.2901	0.2874	1.009
30000	0.1896	0.0032	0.1928	0.1923	1.003
100000	0.0445	0.0006	0.0451	0.0455	0.991

Based on this and other comparisons, the ANS 5.1 Committee issued a position statement to NRC that the current 20% uncertainty in the decay heat standard is a 4 to 8σ value between ~20 and 10^4 s. This position, if legally adopted by NRC, would have important economic implications for most light water reactors. The position followed from a discussion of the following excerpt taken from a review of recent LASL results:

"At the April 8, 1976 Committee Meeting at EPRI, there was a suggestion that the Committee consider 2 standards, 1 for short term heating (≤ 10 000 s) and 1 for longer cooling times. The suggestion was based on the fact, supported by calculations, that short term heating is not significantly effected by neutron absorption and is, therefore, not strongly dependent on the reactor spectrum and irradiation history. The suggestion for two standards, or a division of the standard into two time domains, should be seriously considered by the Committee. It is reasonable because of the physical behavior of the fission products and because uncertainty in the short term heating domain of most immediate (economic) interest can now be reduced. A reduction in uncertainty can be supported by experiments and an analysis of the data in summation calculations. The Committee (ANS 5.1) should consider the utility of an interim standard for short term heating having reduced but conservative uncertainties, with final uncertainties assigned when the results of all current experiments are available.

"For example, the LASL calorimetric experiment indicates that between 20 and 100 000 s, a 2σ uncertainty of 10% is reasonable and conservative (based only on the LASL calorimetric experiment, 10% is close to a 4σ uncertainty). For smaller cooling intervals, a 20% or larger uncertainty (2σ) would apply to the calculated heating rates. (NOTE: The percent energy released during the first 20 s is less than 1% of that released during the first 10 000 s and is ~4.1% of the energy released during the first 1 000 s.)

"The specific suggestion is that:

1. There is enough information to issue an interim standard for short term heating applicable to the LOCA, with reduced, but conservative, uncertainties.
2. The mean value should be generated using ENDF/B-IV data in summation calculations (correcting for at least the ^{98}Zr branching fraction).
3. Final uncertainties and possible changes in the mean value at very short cooling times (< 20s) should await the completion of all experiments.
4. The interim standard can be conservatively based on ^{235}U thermal fission (the ^{239}Pu heating is smaller than the ^{235}U value), or heating from other fuels can be calculated.

5. The actual form and uncertainty assignment of the interim standard, if advisable, should be a committee, not an individual, determination; the result should probably be a simple recommendation to NRC and need not interfere with the work of preparing a final standard."

3. Calculation of Fission Product Concentrations in Spent MTR-Type Fuel for Comparison with Concentrations Determined by Spectral Measurements (G. Hoovler [U. of Virginia], T. R. England, W. B. Wilson, and N. L. Whittemore).

The CINDER-10 code and data set, using processed ENDF/B-IV fission product data, has produced calculated γ spectra in good agreement with spectra measured after relatively short activation and decay times. It would be desirable to compare such spectra with experimental values for activation and decay times exceeding one year.

Experiments involving long irradiation and decay times must necessarily involve a large investment in time and money. Spent MTR-type fuel offers a good fuel sample for spectral examination since irradiation and decay periods are complete. The highly enriched, aluminum-clad fuel is desirable because of the absence of interference from structural material activation. However, flux profile uncertainties, fuel repositioning, and the intermittent operating history typical of research reactors diminish the desired accuracy for many computations.

A fuel element of the University of Virginia Research Reactor is presently being examined. A flux and decay history of the element has been tabulated, and fission product concentrations have been calculated with CINDER-10 and sent to the University of Virginia.

Spectral measurements are in progress at the University of Virginia. Fission product concentrations will be calculated from spectra and compared with CINDER-10 values.

B. Burnup Calculations (M. G. Stamatelatos, T. R. England, and N. L. Whittemore)

Two-group, core-averaged burnup calculations are being made for standard 3000 MW(t) HTGR beginning-of-life to end-of-equilibrium cycle configurations (including fuel reloading) using the CINDER-10 computer code. The thorium and uranium target paths used for the actinide chains are shown in Fig. 31. Linearized chains, required by CINDER-10, were constructed to account for actinide concentrations from ^{232}Th to ^{244}Cm. The cross-section data for the most important actinides (^{232}Th, ^{233}U, ^{234}U, ^{235}U, ^{236}U, ^{238}U, ^{233}Pa, ^{238}Pu, ^{239}Pu, ^{240}Pu, and ^{241}Pu)

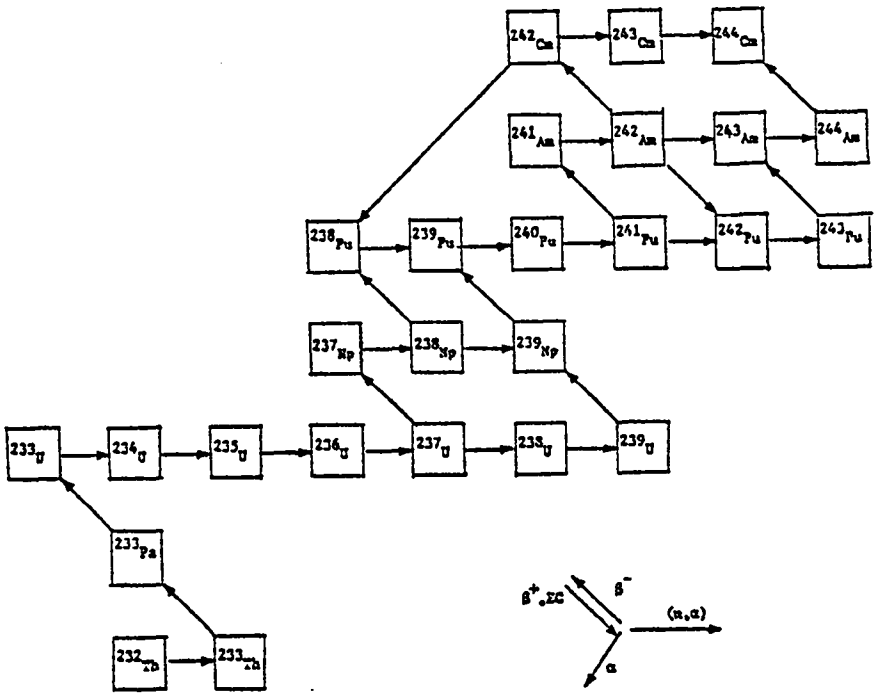

Fig. 31.
Actinides in HTGR burnup calculations.

and for the 2 most important fission products ^{135}Xe and ^{149}Sm) have been obtained by collapsing an existing LASL 9-group ENDF/B-based HTGR cross-section library. The up-to-date ENDF/B-V cross-section data on the remaining actinides have just become available at LASL. Cross section, yield, and other data for the fission products are based on the most recent ENDF/B-IV files. The actinides of Fig. 31 are also being incorporated into burnup calculations for other fuels.

C. EPRI-CINDER and Thermal Reactor Absorption Chain Library (T. R. England, W. B. Wilson, M. G. Stamatelatos, and N. L. Whittemore)

Code modifications, data libraries, survey, and data testing calculations are complete. Two reports in the Electric Power Research Institute (EPRI) format are being prepared. All data are processed from ENDF/B-IV. Cross sections in four energy groups, were averaged in a typical LWR spectrum as described in previous progress reports. A reduced chain set plus a lumped, or fictitious, chain have also been generated for use in spatial depletion calculations.

D. Approximations to Summation Code Results of Delayed Energy and Spectra from Fission Products (R. J. LaBauve, T. R. England, and M. G. Stamatelatos)

ENDF/B-IV fission product data were used as input to a code system consisting of CINDER-10 plus auxiliary codes to calculate photon and β^- spectra emitted by fission products from thermal fission of ^{235}U and other fissionable nuclides, from the instant of a very short fission burst to times up to 10^{13} s.[33-35] This code system is illustrated in Fig. 32 and success has been achieved in using it to compare with recent unreported LASL experiments.[36,37] Also, γ and β^- fission-product spectra from fast and thermal fission of ^{235}U and other fissile and fertile isotopes have been calculated in detailed energy structures (150 equal-grid groups for photons and 75 equal-grid groups for β^-) at several cooling instants per time decade from 0.1 to 10^{13}s.

The considerable amount of data included in these calculations as well as the long computer time and sizeable computer storage required makes it desirable to attempt simple analytical fits to the results of these calculations. In this way (1) spectra for additional intermediate cooling times can be rapidly interpolated and, more importantly (2) an analytical representation of a reactor power history can be folded with the fitted burst function and integrated to give decay spectra at specific cooling times for a given irradiation history.

To date we have demonstrated that a "broad-group" energy representation of the spectral data can be approximately fit with a sum of exponential functions so that when they are folded with a histogram representative of a power history, new analytic functions result that can be easily integrated.

The method used[38] in fitting the calculated data is as follows: We assume the burst function fc(t) for a particular energy group to be a linear combination of functions

$$fc(t) = \sum_{k=1}^{L} \alpha_k g_k(t) \quad , \tag{10}$$

where $g_k(t)$ can be any function but, to date, we are using $g_k(t) = e^{-\lambda_k t}$. The λ_k's are to be chosen by some consistent method but are not fitted; that is, the method we are describing is a linear fit, a fit of the α_k's with adequately chosen λ_k's. It should be noted that we have recently made α and λ fits of functions of this type for the total fission-product decay power following

^{235}U and ^{239}Pu fission bursts. This previous work has given us insight into choosing the λ's for this single parameter fit.

In order to demonstrate the feasibility of this method a small code, ERDALEW, was written to fit calculated fission-product gamma-decay power following a ^{235}U thermal fission burst. An 8-group energy structure shown in Table VIII was arbitrarily chosen for this test case and 2 points per decade from 0.1 to 10^9 s were chosen for the α_k fit.

Results of this test case are shown in Figs. 33-40. It can be seen from these figures that all fits are generally good except for group 7 in the vicinity of 10^5 s where growth reverses the slope of the decay curve.

The fitted burst function can also be folded with a reactor power history so that decay spectra from irradiated fuel can be calculated as a function of cooling time. A small program, CALDEGS, was written to implement the burst function to decay power following extended fuel irradiation. The method was checked by comparing with CINDER-10 integrated spectrum calculations[39] (without neutron absorption) for gamma-decay power, beta-decay power, and gamma- plus beta-decay power after 20 000-h constant power irradiation.

The first step in the fitting procedure was to fit the ^{235}U thermal fission burst decay curves with the ERDALEW code. Results are shown in Figs. 41-43. Because of the sharp change in slope at 5×10^{10} s, a 2-segment fit was required that caused some error in the region of 10^{10} s where the segments joined.

Next, the CALDEGS code was used to calculate the decay curves after 20 000 h constant power irradiation time. Results are shown in Figs. 44-46. Again, the greatest deviation is in the vicinity of 10^{10} s where the 2 fitted burst segments were joined. Such calculations, using the fitted exponentials, are roughly equivalent to calculating a single three-nuclide chain (or less, because nuclide cross sections and decay energies are not involved). The required storage is negligible and such fits can be used in spatial calculations.

Equation (10) permits general functions, $g_k(t)$; therefore, these techniques can also be applied to reduce experimental results to a burst function basis, and thereby enable one to compare results of different experiments. Current decay heat and spectral measurements are made following a short irradiation time, which can be assumed to have a constant fission rate, and analytic functions have been derived for fitting or parameterizing experimental data in terms of equivalent burst functions [Eq. (10)]. Work to analyze several experiments with this technique is in progress at Hanford Engineering Development Laboratory (HEDL) and LASL.

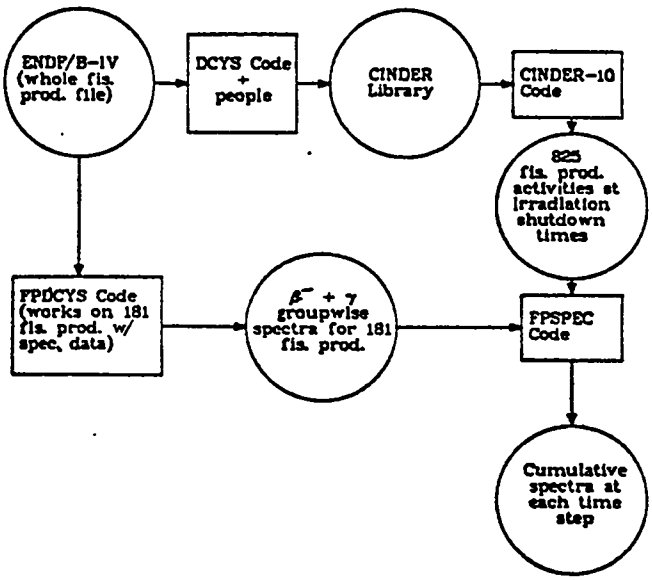

Fig. 32.
LASL code system for producing β^- and γ fission product spectra.

TABLE VIII

EIGHT GROUP ENERGY STRUCTURE USED IN SAMPLE

Group No.	Lower Energy Boundary (MeV)	Upper Energy Boundary (MeV)
1	0.00	0.25
2	0.25	0.50
3	0.50	0.75
4	0.75	1.00
5	1.00	1.50
6	1.50	2.50
7	2.50	4.00
8	4.00	7.50

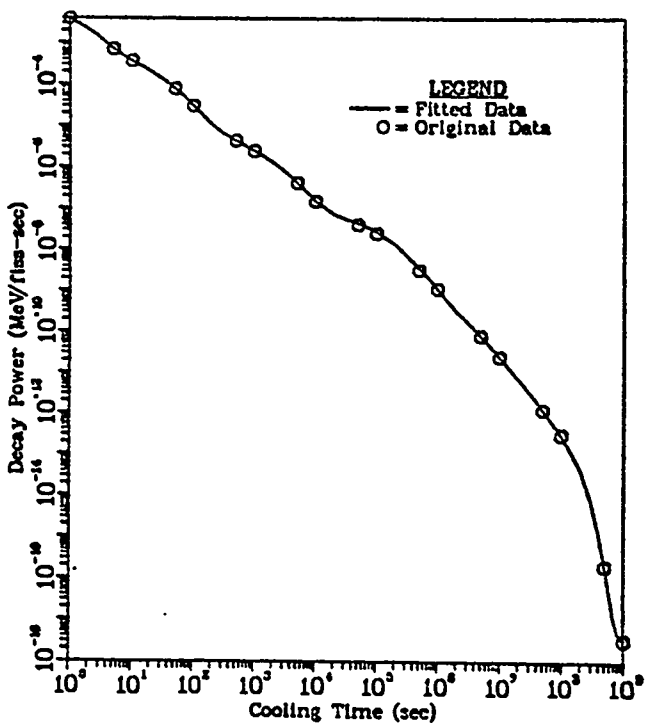

Fig. 33.
Gamma decay power following ^{235}U thermal fission burst for group 1 energy range 0.0 to 0.25 MeV.

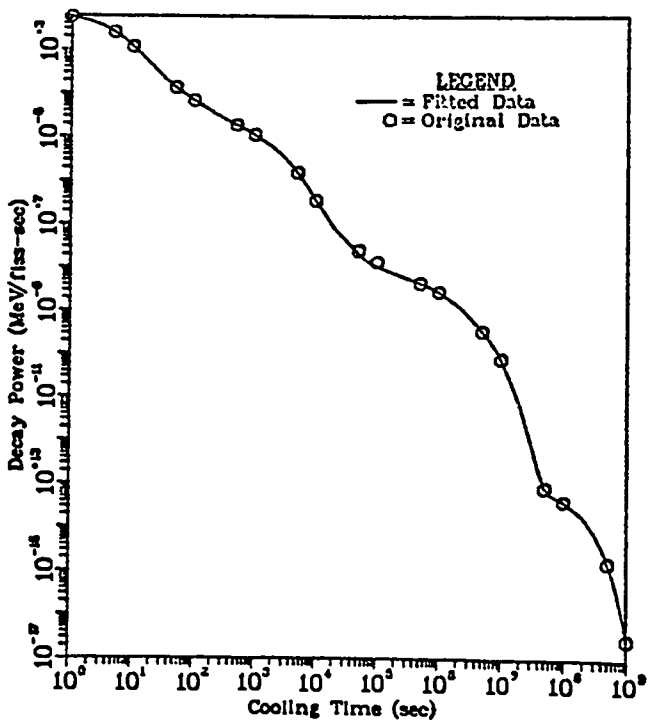

Fig. 34.
Gamma decay power following ^{235}U thermal fission burst for group 2 energy range 0.25 to 0.5 MeV.

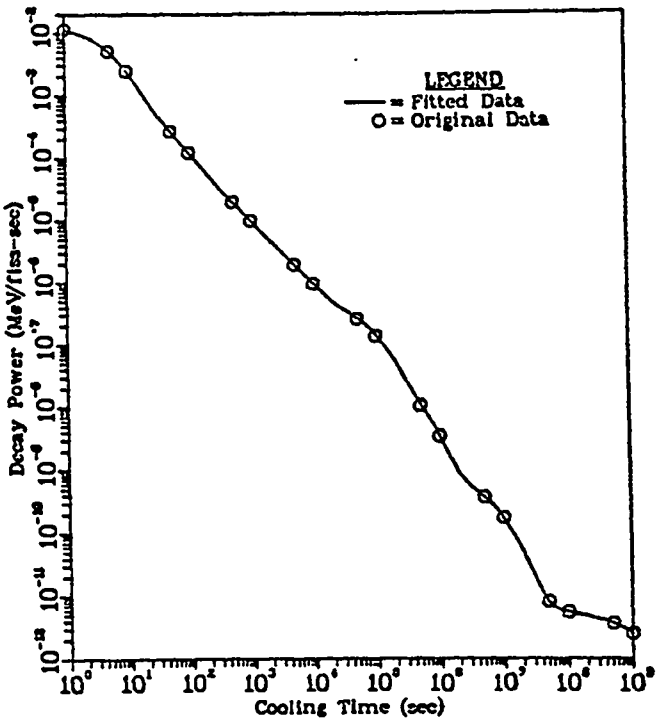

Fig. 35.
Gamma decay power following ^{235}U thermal fission burst for group 3 energy range 0.5 to 0.75 MeV.

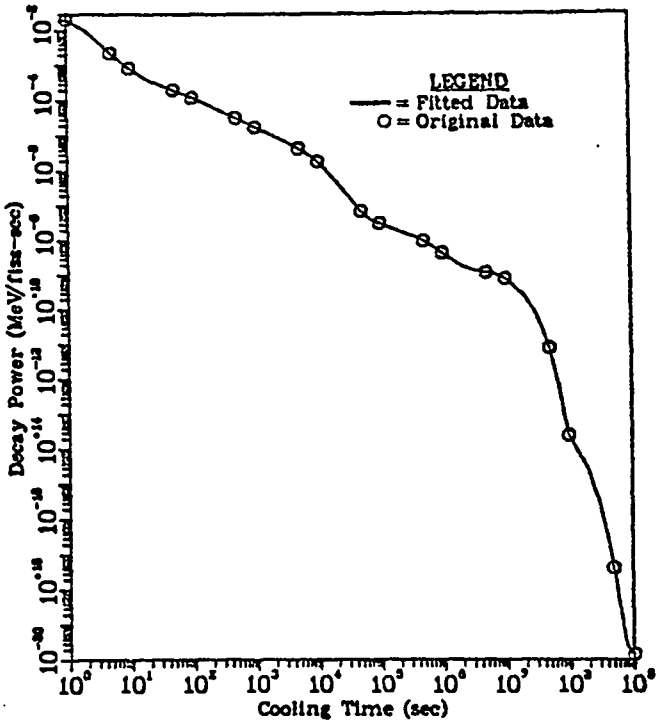

Fig. 36.
Gamma decay power following ^{235}U thermal fission burst for group 4 energy range 0.75 to 1.0 MeV.

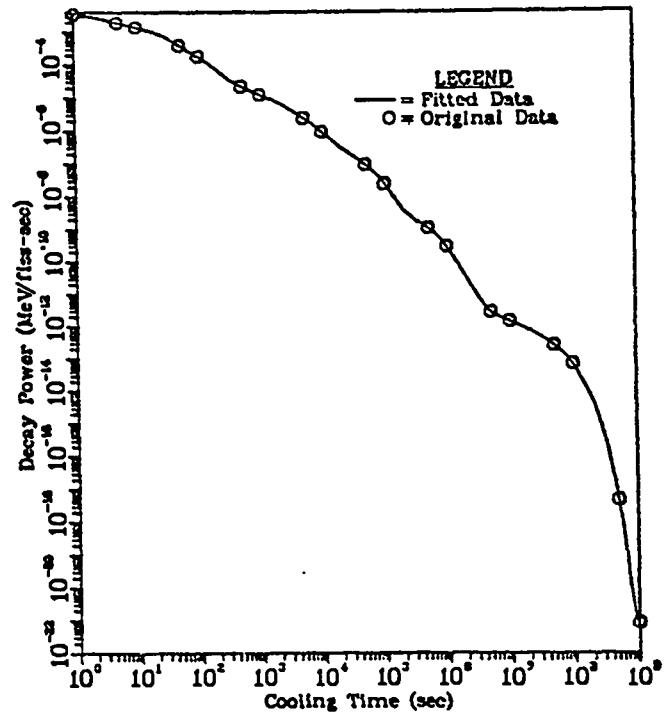

Fig. 37.
Gamma decay power following ^{235}U thermal fission burst for group 5 energy range 1.0 to 1.5 MeV.

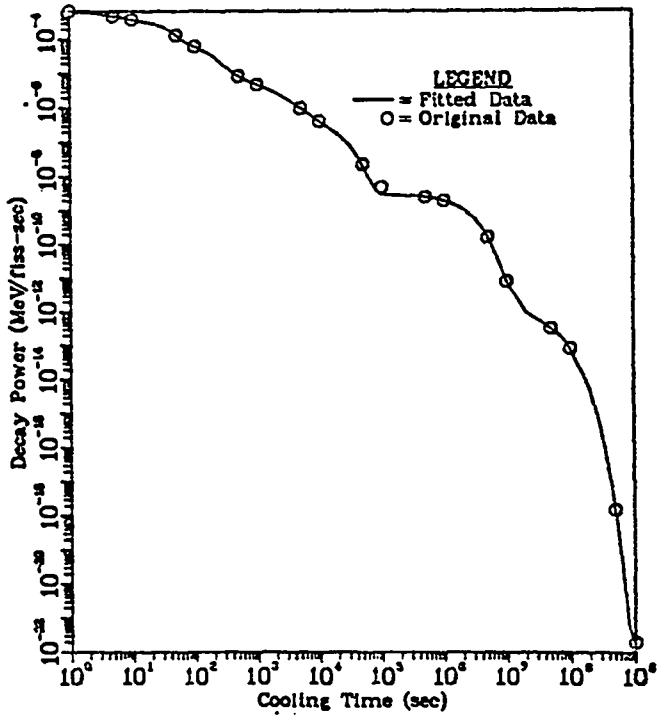

Fig. 38.
Gamma decay power following ^{235}U thermal fission burst for group 6 energy range 1.5 to 2.5 MeV.

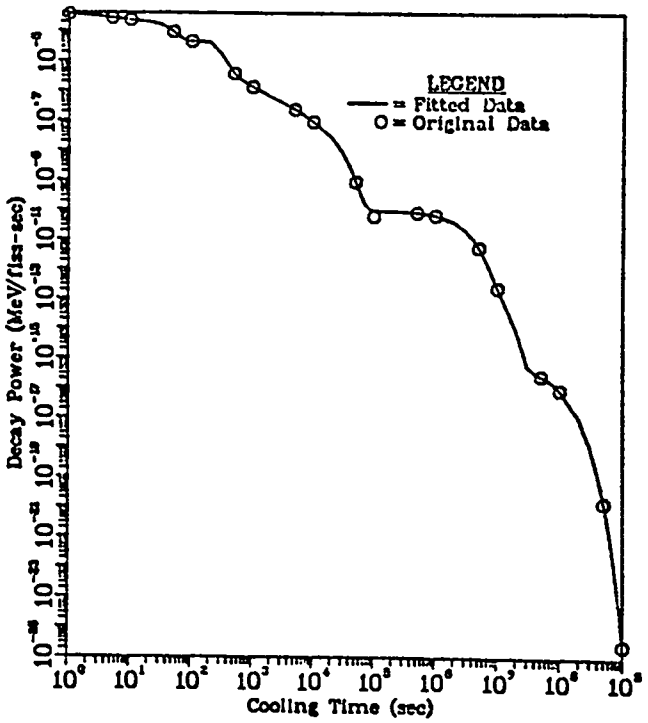

Fig. 39.
Gamma decay power following ^{235}U thermal fission burst for group 7 energy range 2.5 to 4.0 MeV.

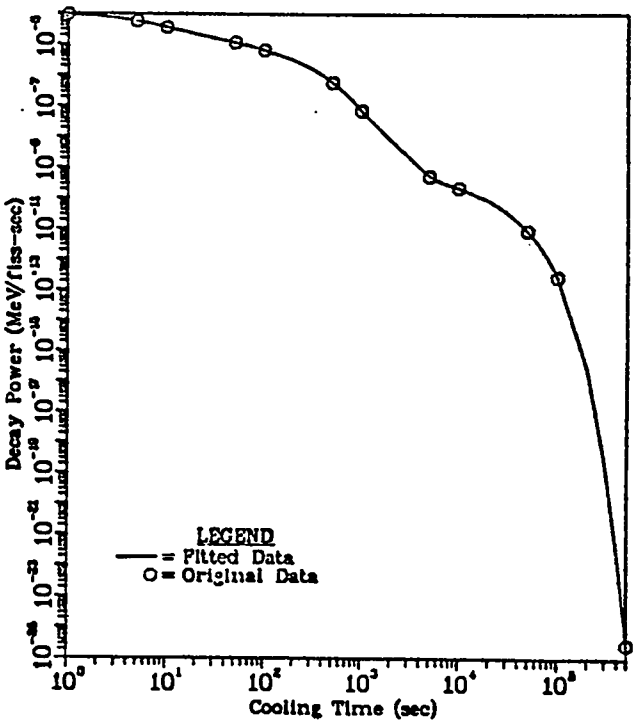

Fig. 40.
Gamma decay power following ^{235}U thermal fission burst for group 8 energy range 4.0 to 7.5 MeV.

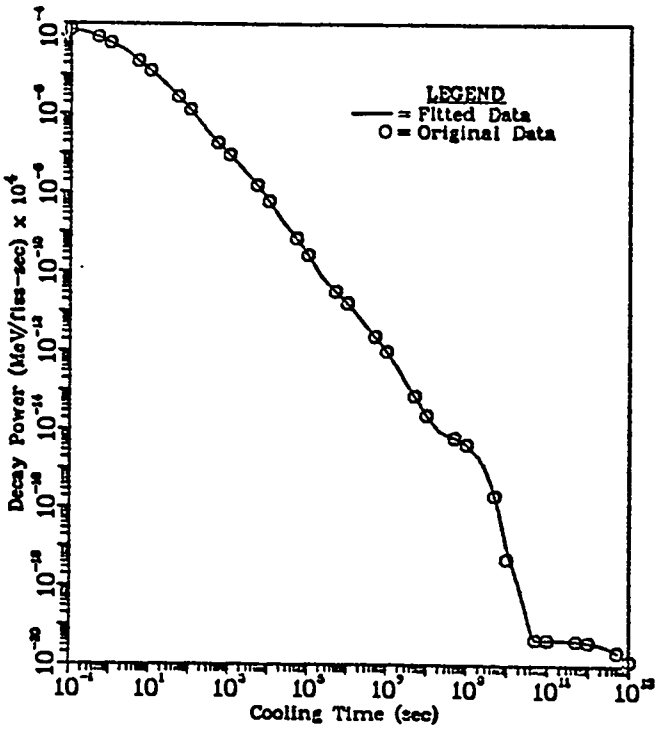

Fig. 41.
Total decay power from ^{235}U thermal burst (gammas and beta -).

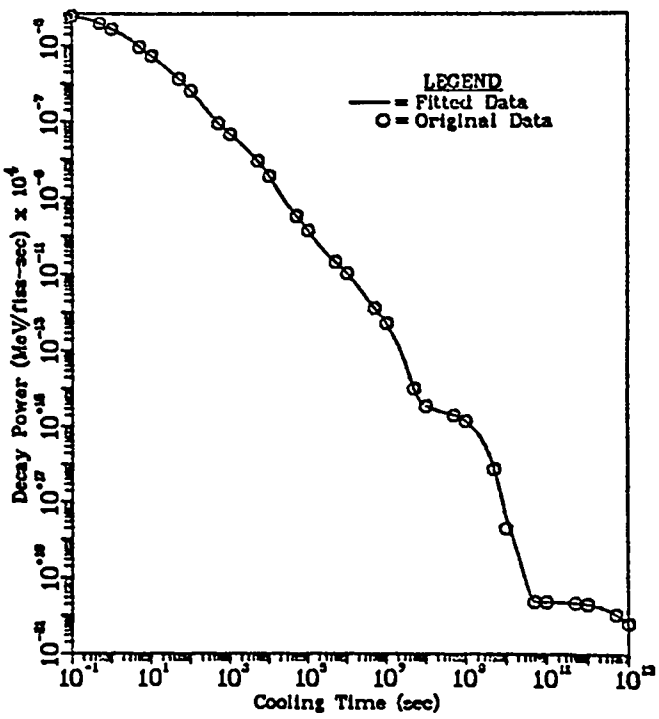

Fig. 42.
Total decay power from ^{235}U thermal burst (gammas only).

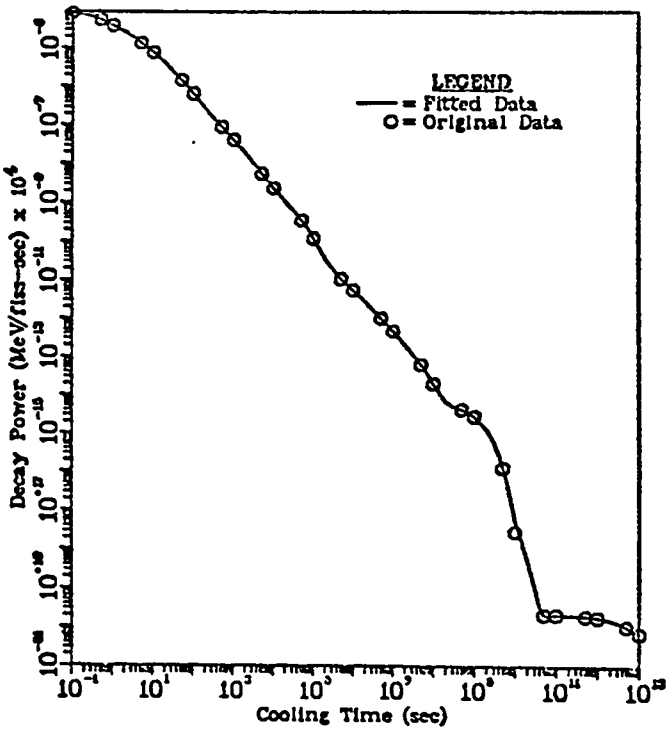

Fig. 43.
Total decay power from ^{235}U thermal burst (beta- only).

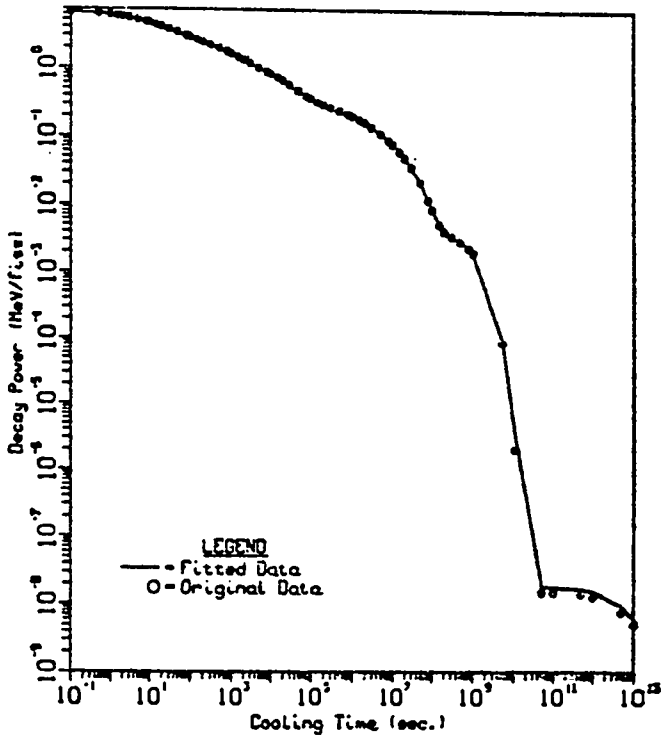

Fig. 44.
Total fission-product decay power from ^{235}U thermal fission after 20 000-h irradiation time (beta- only).

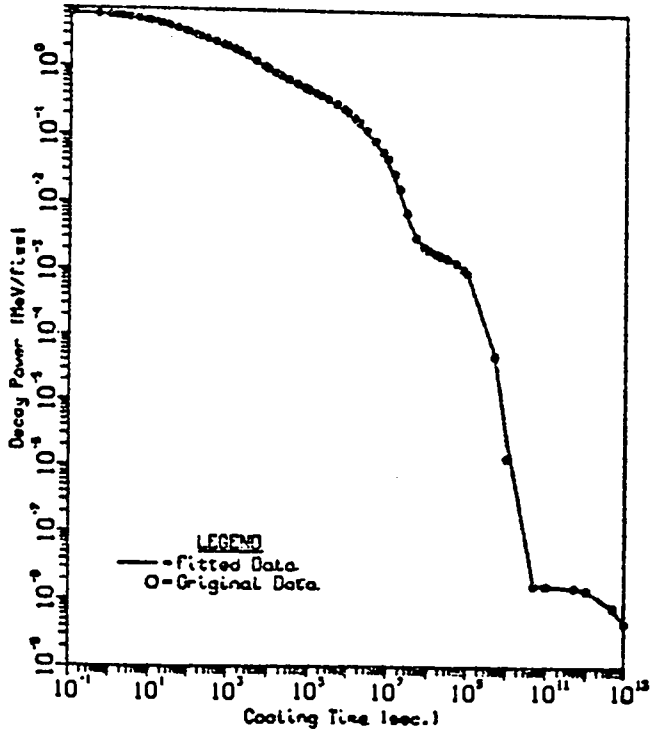

Fig. 45.
Total fission-product decay power from ^{235}U thermal fission after 20 000-h irradiation time (gammas only).

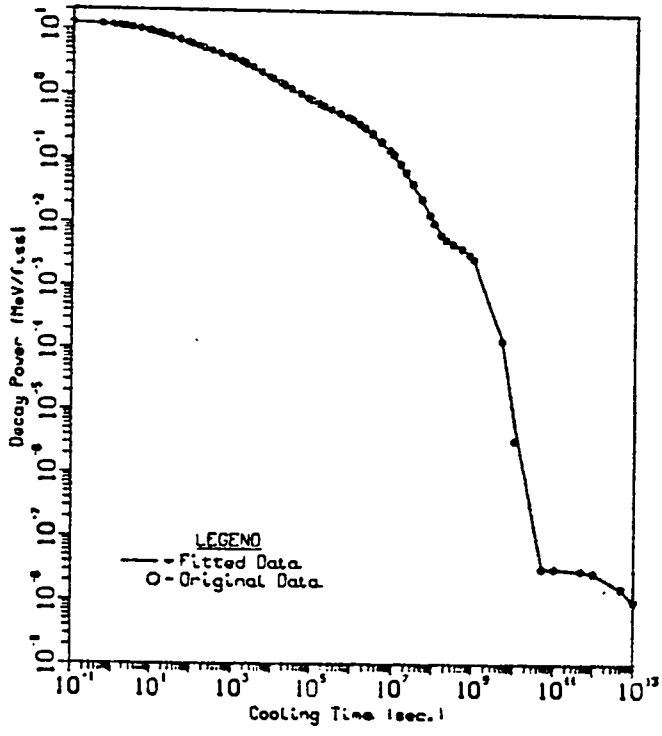

Fig. 46.
Total fission-product decay power from ^{235}U thermal fission after 20 000 h (gammas and beta-).

E. ENDF/B Phenomenological Yield Model Improvements (D. G. Madland and T. R. England)

1. Distribution of Independent Fission-Product Yields to Isomeric States.

The work in preparation for Version V of ENDF/B has been completed. A total of 432 cases, at three neutron energies, has been calculated. A detailed summary, together with a table of calculated branching ratios, is contained in a recent report.[40] A paper on this topic will be presented at the American Nuclear Society International Conference on World Nuclear Power in Washington, D. C. in November 1976.

2. Pairing Effects on the Distribution of Fission-Product Yields.

The work on pairing effects has also been completed. Averaged proton and neutron pairing enhancements to independent yield strengths have been calculated for neutron-induced fission of 17 actinide nuclei, at 7 values of the neutron energy. A detailed summary, together with a table of the calculated proton and neutron pairing enhancements, is contained in a recent report.[41] A paper on this topic will be submitted to the Physical Review. A summary will be presented at the American Nuclear Society International Conference on World Nuclear Power in Washington, D. C. in November 1976.

3. Zp Values for Neutron-Induced Fission.

A study is underway as to how one best extrapolates the most probable charge values (Zp values of the phenomenological model) in ^{235}U thermal fission, for example, to other fissionable nuclides and/or other neutron energies. An attempt is being made to construct a model which simultaneously fits all existing good-quality data, using the restriction that the Gaussian width σ remains constant. If this fails, σ will be given an as yet undetermined parametric dependence.

F. Fission Yield Theory (D. G. Madland, R. E. Pepping [U. of Wisconsin], C. W. Maynard [U. of Wisconsin], and T. R. England)

Current work is addressed to the determination of the most realistic scission configuration. The collective excitations (responsible for the energy dependence of the fragment shapes) are believed to be understood and have been incorporated. A routine has been developed to calculate the Coulomb energy, immediately post-scission, for highly deformed fragments (the multipole expansion is to order 8). The next step will be to calculate yields, however crudely, using a simple level density prescription to study qualitatively the yield dependence upon the assumed scission configuration.

V. MEDIUM ENERGY LIBRARY (D. G. Foster, Jr. and H. M. Holleman)

All of the medium-energy library tapes have now been transferred to photostore. For neutrons incident on ^{238}U, only enough histories were kept to fill one box of photostore at each incident energy.

Work has continued on NASIG, the program to convert data in the NASA equiprobability-mesh format calculated by NASPRO into differential cross sections at arbitrary points. For each incident energy and for each of five secondary particles (n,p,π^+,π^0,π^-) NASPRO divides the cosine μ of the angle between incident and secondary particle into ten columns of unequal width, each containing equal numbers of Monte Carlo histories. Each cosine column is then subdivided into 40 equally probable rectangular blocks along the secondary-energy axis E' = E(secondary)/E(incident). The differential cross section averaged over each block is inversely proportional to its area, and all blocks have the same fractional uncertainty.

The purpose of NASIG is to derive point differential cross sections by fitting a local smoothing function to the cross sections integrated over a cluster of these irregular rectangular blocks. Initially we have chosen a polynomial function of second degree in μ and E', whose six coefficeints are determined by weighted least-squares fitting.

Early versions of NASIG used elementary procedures for determining which blocks from the irregular rectangular grid to use for determining the fit at a particular point (μ,E'). As happens with any running fit, the fitted cross sections jumped erratically as blocks were added to or eliminated from the fit. The angular distribution of secondary nucleons is so strongly forward-peaked above a few hundred-MeV incident energy that one cosine bin covers the entire backward hemisphere. Accordingly, it is not surprising that fitted cross sections frequently went negative at back angles and near the kinematic cutoff energy for all angles.

During the past quarter we have concentrated on minimizing the twin problems of erratic jumps and negative cross sections. Since calculated values will ultimately be required for thousands of points (μ,E'), we assume that a workable solution must be found that requires a minimum of intervention by the user of NASIG. Not surprisingly, the result is that more code is required to select the blocks to be fitted than to complete the fit. The key concepts which we have exploited are these:

1. Erratic jumps can be minimized by keeping the number of blocks being fitted large (10 to 30 out of 400 altogether), and by forcing blocks to be added or dropped one-by-one instead of in clusters.
2. The blocks chosen should be "near" (μ,E') in a coordinate system in which the nearby grid is approximately "square".
3. Points near the edges of the available μ-E' space should use the same cluster of fitted blocks as points somewhat farther from the boundary.
4. The tendency towards negative cross sections near boundaries can be controlled by constraining the fit to have the correct behavior at the boundaries.

We have worked out the computational procedures for constraining the fit in value or directional derivative. They turn out to be surprisingly simple. At the same time, however, it has become clear that parts of the distribution are too complicated for a quadratic surface to give a satisfactory fit. Accordingly, we have derived the design matrix for a third-degree surface.

The block-selection algorithms that appear most promising begin with a "seed" which contains the minimum number of blocks necessary for a stable fit. This seed is then allowed to "grow" by adding blocks that are "near" it in the sense of (2) and (3) above. Growth stops when a specified distance (e.g., $\sqrt{3}$ normalized block-widths) is reached, unless terminated earlier by an arbitrary limit to the number of blocks. This arbitrary limit must be larger near boundaries than in the interior. Fig. 44 shows an example of the result of such a selection process.

Development of NASIG has been halted by loss of funding. The principal task remaining is to explore the boundary-constraint procedures in detail.

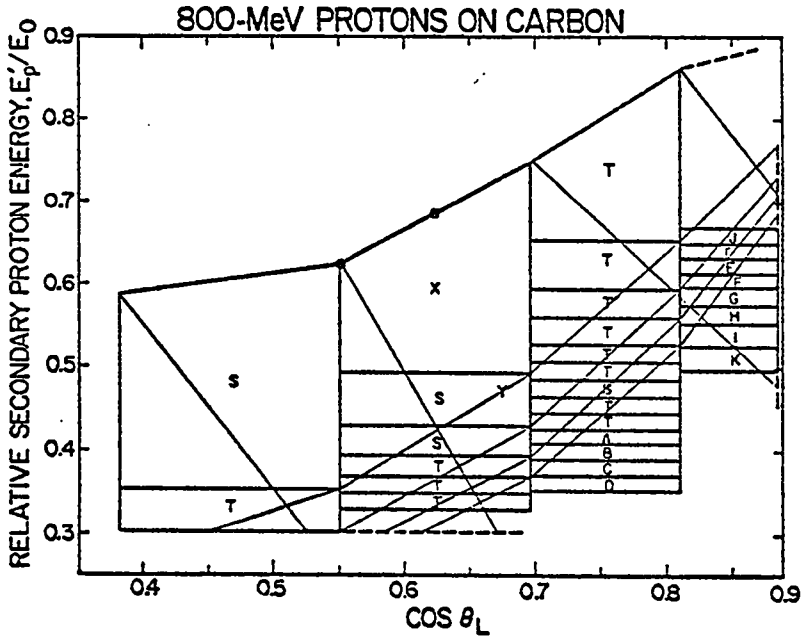

Fig. 44.
An example of the block-selection process. For a fit at X the blocks are chosen initially as if it were at Y. "Seed" blocks are marked S. Blocks marked T are added next because of proximity to the upper boundary. Blocks A through D are added because they are "near" Y in its local coordinate system, and E through K because they are "near" X in its own coordinate system. Sloping lines define "pseudorows" and "pseudocolumns" useful in selecting the T blocks. The circles on the top boundary mark points at which the fit will be constrained.

REFERENCES

1. G. M. Hale, J. Devaney, D. C. Dodder, and K. Witte, "An R-Matrix Analysis of the p-^{3}He Scattering Below E_p = 19.5 MeV," Bull. Am. Phys. Soc. 19, 506 (1974).

2. R. F. Haglund, Jr., D. Fick, P. A. Schmelzbach, G. G. Ohlsen, N. Jarmie, and R. A. Brown, "^{1}H(t,t)^{1}H Scattering at Low Energies," Bull. Am. Phys. Soc. 21, 989 (1976); and private communication.

3. E. D. Arthur and P. G. Young, "A New Statistical-Preequilibrium Nuclear Model Code," Trans. Am. Nucl. Soc. 23, 500 (1976).

4. G. J. Pyle, "RAROMP (Regular and Reformulated Optical Model Potential)," John H. Williams Laboratory of Nuclear Physics Internal report, University of Minnesota (private communication) (1968).

5. D. M. Drake, G. F. Auchampaugh, E. D. Arthur, C. E. Ragan, and P. G. Young, "Double-Differential Beryllium Neutron Cross Sections at Incident Neutron Energies of 5.9, 10.1, and 14.2 MeV," Los Alamos Scientific Laboratory report LA-6257 (August 1976).

6. D. I. Garber and R. R. Kinsey, "Neutron Cross Sections, Vol. II," Brookhaven National Laboratory report BNL 325, 3rd Ed. (Jan 1976).

7. G. Haouat, J. Lachkar, J. Sigaud, Y. Patin, and F. Cocu, "Differential Cross Sections for Carbon Neutron Elastic and Inelastic Scattering from 8.0 to 14.5 MeV," Centre d'Etudes de Bruyéres-le-Châtel report CEA-R-4641 (Feb. 1975).

8. B. A. Watson, P. D. Singh, and R. E. Segel, "Optical Model Analysis of Nucleon Scattering from 1-p Shell Nuclei between 10 and 50 MeV," Phys. Rev. 182, 1977 (1969).

9. F. D. Becchetti, Jr., University of Michigan (private communication).

10. H. Rebel and G. W. Schweimer, "Improved Version of Tamura's Code for Coupled Channel Calculations: JUPITOR Karlsruhe Version," Gesellschaft für Kernforschung M.B.H. report KFK 1333 (February 1971).

11. T. Tamura, "Computer Program JUPITOR-1 for Coupled Channel Calculations," Oak Ridge National Laboratory report ORNL-4152 (August 1967).

12. P. G. Young and D. G. Foster, Jr., "A Preliminary Evaluation of the Neutron and Photon-Production Cross Sections for Aluminum," Los Alamos Scientific Laboratory report LA-4726(ENDF-175) (1972).

13. R.E. MacFarlane, R. M. Boicourt, R. J. Barrett, and H. M. Holleman, "NJOY Code Development," in "Applied Nuclear Data Research and Development October 1 - December 31, 1975," Los Alamos Scientific Laboratory report LA-6266-PR (1976), p. 4.

14. S. A. W. Gerstl, D. J. Dudziak, and D. W. Muir, "Cross Section Sensitivity and Uncertainty Analysis with Application to a Fusion Reactor," Nucl. Sci. Eng. 62, 137 (1977).

15. Y. D. Naliboff and J. U. Koppel, "HEXSCAT, Coherent Elastic Scattering of Neutrons by Hexagonal Lattices," General Atomic report GA-6026 (1964).

16. C. I. Baxman, G. M. Hale, and P. G. Young, "Applied Nuclear Data Research and Development January 1 - March 31, 1976," Los Alamos Scientific Laboratory report LA-6472-PR (August 1976).

17. J. U. Koppel and D. H. Houston, "Reference Manual for ENDF Thermal Neutron Scattering Data," General Atomic report GA-8774 (1968).

18. M. K. Drake, "Data Formats and Procedures for the ENDF Neutron Cross Section Library," Brookhaven National Laboratory report BNL-50274 (ENDF 102) (1970).

19. EPRI-CELL, GAMTAP, and LIBRAR are proprietary products of Nuclear Associates International Corp., 6003 Executive Blvd., Rockville, Md. 20852.

20. C. I. Baxman and P. G. Young, "Applied Nuclear Data Research and Development April 1 - June 30, 1976," Los Alamos Scientific Laboratory report LA-6560-PR (Nov. 1976).

21. W. W. Clendenin, "Calculation of Thermal Neutron Scattering Cross Sections for Crystalline Materials: The TOR Program," Los Alamos Scientific Laboratory report LA-3823 (1967).

22. J. V. Koppel, J. R. Triplett, and Y. D. Naliboff, "GASKET, A Unified Code for Thermal Neutron Scattering," General Atomics report GA-7417 (1966).

23. W. W. Clendenin, "Calculation of Thermal Neutron Diffusion Length and Group Cross Sections: The GLEN Program," Los Alamos Scientific Laboratory report LA-3893 (1968).

24. A. T. D. Butland, "LEAP and ADDELT, A Users Guide to Two Complementary Codes on the ICL-470 for Calculating the Scattering Law from a Photon Frequency Function," Atomic Energy Establishment Winfrith report AEEW-M 1200 (1973).

25. R. B. Kidman, "240-Group Library (LIB-IV-240)," in "Applied Nuclear Data Research and Development January 1 - March 31, 1976," Los Alamos Scientific Laboratory report LA-6472-PR (1976), p. 24.

26. F. W. Brinkley and G. E. Bosler, private communication.

27. T. R. Hill, "ONETRAN: A Discrete Ordinates Finite Element Code for the Solution of the One-Dimensional Multigroup Transport Equation," Los Alamos Scientific Laboratory report LA-5990-MS (1975).

28. H. Alter, R. B. Kidman, R. J. LaBauve, R. Protsik, and B. A. Zolotar, "Cross Section Evaluation Working Group Benchmark Specifications," Brookhaven National Laboratory report BNL-19302 [ENDF-2022] (Nov. 1974).

29. R. W. Hardie and W. W. Little, Jr. "1DX, A One-Dimensional Diffusion Code for Generating Effective Nuclear Cross Sections," Battelle Northwest Laboratory report BNWL-954 (March 1969).

30. R. W. Hardie and W. W. Little, Jr., "PERT-V, A Two-Dimensional Perturbation Code for Fast Reactor Analysis," Battelle Northwest Laboratory report BNWL-1162 (1969).

31. W. W. Little and R. W. Hardie, "2DB User's Manual — Revision 1," Battelle Northwest Laboratory report BNWL-831, Rev. 1 (Aug. 1969).

32. N. Tsoulfanidis, B. W. Wehring, and M. E. Wyman, "Measurements of Time-Dependent Energy Spectra of Beta Rays from Uranium-235 Fission Fragments," Nucl. Sci. and Eng. 43, 42 (1971).

33. T. R. England, R. E. Schenter, and N. L. Whittemore, "Gamma and Beta Decay Power Following ^{235}U and ^{239}Pu Fission Bursts," Los Alamos Scientific Laboratory report LA-6021-MS (July 1975).

34. M. G. Stamatelatos and T. R. England, "Beta-Energy Averaging and Beta Spectra," Los Alamos Scientific Laboratory report LA-6445-MS (ENDF-242) (August 1976).

35. T. R. England and M. G. Stamatelatos, "Beta and Gamma Spectra and Total Decay Energies from Fission Products," Trans. Am. Nucl. Soc. 23, 493 (1976); M. G. Stamatelatos and T. R. England, "Method for Calculating Average Beta Energies and Beta Spectral Shapes," Trans. Am. Nucl. Soc. 23, 502 (1976); and D. G. Foster, Jr. and T. R. England, "Time-Dependent Spectra of Photons and Spontaneous-Fission Neutrons for Applied Problems," Trans. Am. Nucl. Soc. 23, 551 (1976).

36. E. Jurney, Los Alamos Scientific Laboratory, private communication (1976).

37. J. Yarnell, Los Alamos Scientific Laboratory, private communication (1976).

38. R. E. Schenter, Hanford Engineering Development Laboratory, private communication (1976).

39. T. R. England, Los Alamos Scientific Laboratory, private communication (1976).

40. D. G. Madland and T. R. England, "Distribution of Independent Fission-Product Yields to Isomeric States," Los Alamos Scientific Laboratory report LA-6595-MS [ENDF-241] (1976).

41. D. G. Madland and T. R. England, "The Influence of Pairing on the Distribution of Independent Yield Strengths in Neutron-Induced Fission," Los Alamos Scientific Laboratory report LA-6430-MS [ENDF-240](July 1976).